scientific reports

Check for updates

OPEN

Gelatin/PLA-loaded gold nanocomposites synthesis using *Syzygium cumini* fruit extract and their antioxidant, antibacterial, anti-inflammatory, antidiabetic and anti-Alzheimer's activities

Manickam Rajkumar[1], S. I. Davis Presley[1]✉, Nathiya Thiyagarajulu[2], Koyeli Girigoswami[3,4]✉, Gopalarethinam Janani[3], Chinnaperumal Kamaraj[5], Bharathi Madheswaran[6], Bhupendra Prajapati[7], Nemat Ali[8] & Mohammad Rashid Khan[8]

Nanotechnology has experienced significant advancements, attracting considerable attention in various biomedical applications. This innovative study synthesizes and characterizes Ge/PLA/AuNCs (gelatin/PLA/gold nanocomposites) using *Syzygium cumini* extract to evaluate their various biomedical applications. The UV–Visible spectroscopy results in an absorption peak at 534 nm were primarily confirmed by Ge/PLA/AuNCs synthesis. The FTIR spectrum showed various functional groups and the XRD patterns confirmed the crystalline shape and structure of nanocomposites. The FESEM and HRTEM results showed a oval shape of Ge/PLA/AuNCs with an average particle size of 21 nm. The Ge/PLA/AuNC's remarkable antioxidant activity, as evidenced by DPPH (70.84 ± 1.64%), ABTS activity (86.17 ± 1.96%), and reducing power activity (78.42 ± 1.48%) at a concentration of 100 µg/mL was observed. The zone of inhibition against *Staphylococcus aureus* (19.45 ± 0.89 mm) and *Echericia coli* (20.83 ± 0.97 mm) revealed the excellent antibacterial activity of Ge/PLA/AuNCs. The anti-diabetic activity of Ge/PLA/AuNCs was supported by inhibition of α-amylase (82.56 ± 1.49%) and α-glucosidase (80.27 ± 1.57%). The anti-Alzheimer activity was confirmed by inhibition of the AChE (76.37 ± 1.18%) and BChE (85.94 ± 1.38%) enzymes. In vivo studies of zebrafish embryos showed that Ge/PLA/AuNCs have excellent biocompatibility and nontoxicity. The SH-SY5Y cell line study demonstrated improved cell viability (95.27 ± 1.62%) and enhanced neuronal cell growth following Ge/PLA/AuNCs treatment. In conclusion, the present study highlights the cost-effective and non-toxic properties of Ge/PLA/AuNCs. Furthermore, it presents an attractive and promising approach for various future biomedical applications.

Keywords Nanocomposite, *Syzygium cumini*, Antioxidants, Anti-diabetic, Anti-Alzheimer's

[1]Department of Chemistry, Sri Sivasubramaniya Nadar College of Engineering, Chennai, Tamil Nadu 603 110, India. [2]Department of Life Sciences, Kristu Jayanti College, Bengaluru, Karnataka 560 077, India. [3]Faculty of Allied Health Sciences, Chettinad Hospital and Research Institute, Chettinad Academy of Research and Education, Chennai, Tamil Nadu 603 110, India. [4]Centre for Global Health Research, Saveetha Medical College, Saveetha Institute of Medical and Technical Sciences, Thandalam, Chennai 602101, India. [5]Interdisciplinary Institute of Indian System of Medicine (IIISM), Directorate of Research, SRM Institute Science and Technology, Kattankulathur, Chennai, Tamil Nadu 603 203, India. [6]Department of Pharmaceutical Engineering, Vinayaka Mission's Kirupananda Variyar Engineering College, Ariyanur, Salem, Tamil Nadu 636 308, India. [7]Shree S. K. Patel College of Pharmaceutical Education and Research, Ganpat University, Kherva, Gujarat 384012, India. [8]Department of Pharmacology and Toxicology, College of Pharmacy, King Saud University, 11451 Riyadh, Saudi Arabia. ✉email: davispresleysi@ssn.edu.in; koyelig@gmail.com

Nanotechnology holds immense potential to revolutionize various scientific sectors. Nanomaterials, with their unique morphology and size, offer a wide range of applications and have been the subject of intense research in both biology and material science[1,2]. Nano-sized semiconductors have recently emerged as a novel approach due to their remarkable chemical and physical properties. However, there are some drawbacks associated with this process, such as its high cost, time-consuming nature, and labor-intensive procedures. To overcome these limitations, there is a growing demand for an alternative method that is safe, ecologically sound, and cost-effective for nanoparticle (NP) synthesis[3–5]. In recent years, green synthesis methods have gained popularity. These methods avoid the expensive costs of harsh chemicals as well as the stringent conditions necessary for reduction and stabilization[6].

Green synthesis approaches utilize bacteria, fungi, algae, and plant parts like fruits, stems, roots, leaves, and seed extracts[7,8]. Biosynthetic methods, especially those using plants, are becoming increasingly popular as a streamlined alternative and scalable approach for producing metal oxide particles free of impurities. These biosynthetic techniques produce nanoparticles with more precise shapes and sizes than those achieved through other physicochemical methods[9,10]. Natural compounds found in biological systems play a crucial role in NP synthesis. They serve as capping, reducing, and stabilizing agents. These compounds aid in controlled synthesis and enhance NPs stability. Literature surveys have revealed the significant benefits of employing plants over other biosystems. Moreover, plants are easily accessible, and their NPs are more stable. Furthermore, using plants in biosynthesis presents a sustainable and eco-friendly approach[11,12].

Gold nanoparticles (AuNPs) have gained prominence in recent years due to their enhanced physical, chemical, and biological properties[13]. AuNPs are favored for their ease of production, modification, and properties that depend on size, shape, and dispersion. These factors contribute to the popularity of metal nanoparticles in scientific research and technological advancements[14]. The preferred method for producing AuNPs is green synthesis, which refers to environmentally friendly and biocompatible methods[15]. It aligns with the principles of sustainability and reduces the reliance on harsh chemicals. Medicinal plants and the synthesis of plant-mediated nanomaterials have been thoroughly studied for their ability to synthesize AuNPs. These medicinal plants contain a wide variety of bioactive chemicals possessing well-established therapeutic characteristics[14–16]. Various medicinal plants, such as *Ziziphus nummularia*[17], *Hippeastrum hybridum*[18], and *Ajuga Bracteosa*[19], have been used to synthesize AuNPs in specific studies, highlighting their potential biomedical applications. Additionally, AuNPs have exhibited significant antioxidant, antibacterial, anti-cancer, anti-inflammatory, antidiabetic, and antifungal activities. Their unique properties make them valuable in drug delivery systems and diagnostic tools[19,20].

Gelatin (Ge) is a naturally occurring hydrogel that has reactive amide and amino groups within its structure. Gelatin has been thoroughly investigated as a hydrogel wound dressing owing to its remarkable attributes, such as biodegradability, biocompatibility, adherence, and non-allergenicity[21]. The tissue engineering of gelatin is due to its diverse charged groups, which can engage with both negatively and positively charged elements of cell membranes. Nonetheless, a primary issue associated with gelatin and other natural polymers is their limited stability and diminished mechanical strength in biomedical applications[22]. This limitation hinders their effectiveness as wound dressings and other biomedical products. To address this problem, researchers have explored the incorporation of polylactic acid (PLA) into nanomaterials. PLA is a polymer that offers improved viability, proliferation, and gene expression, thereby enhancing the biocompatibility of electrospun membranes[23]. PLA, being non-toxic, highly crystalline, water-soluble, biodegradable, and highly biocompatible, is widely used as a hydrogel in wound dressing applications. By blending the naturally derived hydrogel gelatin with the synthesized polymer PLA, the stability of hydrogels can be increased, and their physical properties can improve various biomedical properties[23,24]. Blending Ge/PLA binding with metal NPs offers several advantages for ideal tissue engineering, including non-toxicity, antibacterial properties, and wound healing efficiency[25,26].

Recent efforts have focused on designing nanocomposite hydrogels by incorporating drugs of natural origin, primarily derived from plants[27]. *Syzygium cumini* (*S. cumini*) is one such herb that has gained popularity in therapeutic applications, diet based therapy, and contemporary medicine[28]. This herbal plant contains various pharmacological compounds, including sugars, vitamins, enzymes, alkaline, phenolic compounds, glycoproteins and polysaccharides, which contribute to its numerous medicinal properties[29]. Scientific reports have emphasized the pharmacological properties of *S. cumini*, highlighting its potential as an antibacterial, anti-cancer, antioxidant, anti-inflammatory, and wound-healing activity. *S. cumini* is also associated with anti-diabetic properties that help control blood glucose levels and enhance insulin receptor function[29–31]. Notably, researchers have shown the synthesis and various biological applications of *S. cumini* extract, such as silver NPs[32], copper NPs[33], and Zinc oxide NPs[34].

Recent studies have highlighted the potential of synthesized gelatin/AuNPs to exhibit excellent drug delivery and various biological properties[35]. Polymer-loaded NPs have demonstrated high levels of antibacterial activity and controlled drug release properties attributed to the interaction of NPs with bacterial cell membranes, causing alterations and damage to the cellular proteins, DNA, and cell death[35,36]. In a report, the use of *Piper nigrum* extract in the production of AuNPs has demonstrated impressive antibacterial and antioxidant properties[37]. Studies have shown that only a few nanocomposites have been successfully synthesized[35,36]. However, only a few specific nanocomposites synthesized in foliage have been found to have biomedical applications. Cost-effectiveness, non-toxicity, and some significant challenges are observed in nanocomposite synthesis. To the best of our knowledge, the potential of gelatin/PLA-loaded Au nanocomposite (Ge/PLA/AuNCs) and its various biological applications have not been studied. The synthesis of Ge/PLA/AuNCs using the medicinally important *S. cumini* plant extract presents a novel approach with potential clinical applications and describes it as a promising candidate for various biomedical activities. Diabetes, Alzheimer's disease and many other diseases are manifested by oxidative stress, thus highlighting that it may be a promising drug candidate to combat oxidative stress and additionally exhibit antidiabetic and anti-Alzheimer activity.

The novelty of this study is the synthesis of Ge/PLA/AuNCs using *S. cumini* plant fruit extract using the green synthesis method and the aim was to investigate its properties for biomedical applications. The physical and chemical properties of synthesized Ge/PLA/AuNCs were evaluated by UV–vis spectroscopy, FTIR, XRD, SEM, TEM, swelling and drug release properties. The objective is to explore the diverse antioxidant properties of Ge/PLA/AuNCs. Additionally, the research investigates their antibacterial effects against Gram-positive and Gram-negative bacteria. The synthesized Ge/PLA/AuNCs are evaluated for their potential anti-inflammatory, antidiabetic and anti-Alzheimer's activities. The in vivo biocompatibility was also assessed using zebrafish embryos. Furthermore, the study aims to evaluate cell viability and neuroprotective effects by using SH-SY5Y neuroblastoma cell lines.

Results and discussions

UV–visible spectroscopy

The formation of Ge/PLA/AuNCs, achieved by reducing $HAuCl_4$ with *S. cumin* fruit extracts, was primarily confirmed by a notable change in the color of the reaction mixture. This color change serves as a preliminary identification method for the formation of Ge/PLA/AuNCs. What makes the Ge/PLA/AuNCs stand out is their unique colour change from yellow to ruby red, which is caused by surface plasmons within the nanoparticles getting changed. This color transformation was observed for different concentrations of 0.2%, 0.4%, 0.6%, 0.8%, and 1% (Fig. 1a), as well as at various time intervals of incubation (10, 30, 60, 120 and 180 min) (Fig. 1b), with absorbance measurements confirmed at a wavelength of 534 nm.

The absorption intensity increased with higher Ge/PLA/AuNCs concentrations, reaching a maximum value. The presence of various phytochemicals in the plant extract facilitates the oxidation process, leading to the reduction of metal cations into neutral metal atoms. These reduced metal atoms are further stabilized by the bio-ingredients present in the extract, particularly antioxidants such as flavonoids and polyphenols[38]. Their presence

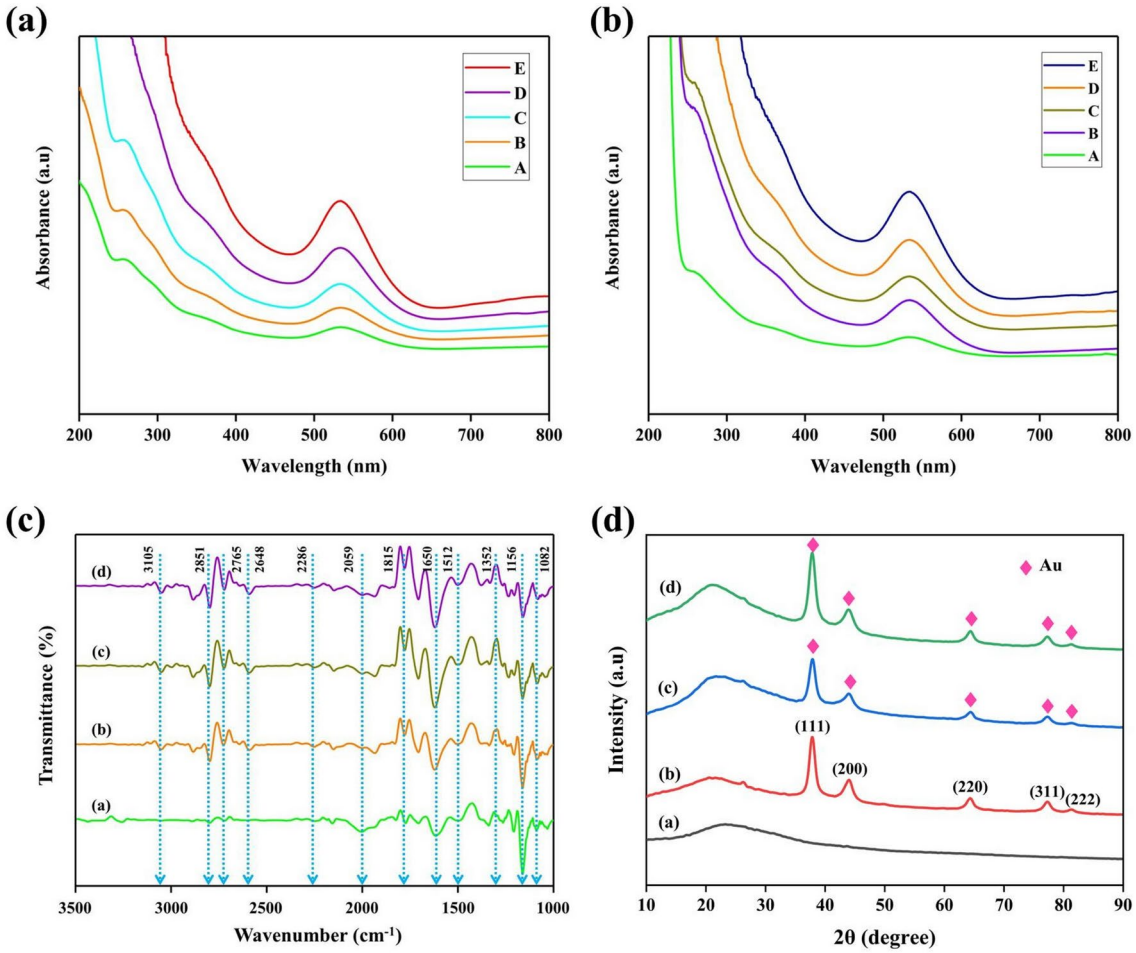

Fig. 1. (**a**) UV–Vis absorption spectra of Ge/PLA/AuNCs synthesized using *Syzygium cumini* extract with different concentrations (A-0.2%, B-0.4%, C-0.6%, D-0.8%, and E-1%) and (**b**) with different time periods (A-10, B-30, C-60, D-120 and E-180 min). (**c**) FTIR spectral analysis of synthesized a) gelatin, (**b**) AuNPs, (**c**) Ge/AuNPs and (**d**) Ge/PLA/AuNCs. (**d**) XRD analysis synthesized a) gelatin, (**b**) AuNPs, (**c**) Ge/AuNPs and (**d**) Ge/PLA/AuNCs.

aids in the simple reduction of gold metal during synthesis. Reports show similar UV–Vis spectrum absorption results at 534 nm when AuNPs were synthesized using *Nigella sativa* plant extract[39].

FTIR analysis

A Fourier-transform infrared spectroscopy (FTIR) analysis was conducted to ascertain the presence of plant phytochemical functional groups in the synthesized Ge/PLA/AuNCs. (Fig. 1c) displays the FTIR spectroscopy profile of Ge/PLA/AuNCs synthesized using *S. cumini* fruit extracts. The FTIR spectrum revealed several characteristic peak values corresponding to different functional compounds present in the extracts. Notably, the medium peak at 3105 cm^{-1} indicated the presence of an O–H stretching mode, suggesting the presence of carboxylic acid in the extracts. When alkanes were present, we observed strong stretching vibration peaks at 2851 cm^{-1} and 2765 cm^{-1} for the C–H group, and 1815 cm^{-1} for the C–O groups. The strong stretching vibration peaks at 1650 cm^{-1} and 1512 cm^{-1} exhibited stretching vibrations of primary and secondary amines and aromatics, indicating the presence of N–H groups and C–C groups attached to the AuNPs[40].

Additionally, sharp peaks at 1352 cm cm^{-1} and 1156 cm cm^{-1} indicated the presence of strong C-H and C-N stretching vibrations, further confirming the presence of plant phytochemical functional groups. The bonds or functional groups derived from heterocyclic compounds, such as alkaloids, flavones, amines, and carboxylic acids, were identified through the presence of C–N and C=C bonds[41]. The proteins present in the fruit extract functioned as capping ligands for the Ge/PLA/AuNCs, as evidenced by the peaks associated with proteins. These protein molecules serve as surface coating molecules, preventing internal agglomeration of the Ge/PLA/AuNCs and enhancing their stability.

XRD analysis

The X-ray diffraction (XRD) analysis was performed to confirm the particle crystalline size, structure, and crystalline phase purity of the synthesized Ge/PLA/AuNCs. (Fig. 1d) displays the XRD pattern of Ge/PLA/AuNCs synthesized using *S. cumini* fruit extracts. The XRD pattern of Ge/PLA/AuNCs exhibited distinct peaks at 38.45°, 44.62°, 64.58°, 77.61° and 82.74° in the 2θ range, corresponding to the (111), (200), (220), (311), and (222) planes, respectively. These peaks are characteristic of the face-centered cubic lattice structure of nanogold. The average crystalline sizes of synthesized Ge/PLA/AuNCs were 22 nm to 67 nm. An important observation is that the most intense peak observed in the synthesized AuNPs using *S. cumini* plant extract was attributed to the (111) plane. This significant finding indicates that the crystals have a preferred orientation toward this particular plane[42]. Therefore, the bio-fabricated Ge/PLA/AuNCs were confirmed to be AuNPs. A recent study also reported similar XRD results for AuNPs synthesized using *Nigella sativa* plant extract[39].

FESEM analysis

Using Field emission scanning electron microscopy (FESEM) to look at Ge/PLA/AuNCs in great detail helped us understand their shape and size. The micrograph revealed the spherical morphology of the Ge/PLA/AuNCs using *S. cumini* plant extract. The FESEM analysis indicated that the Ge/PLA/AuNCs were uniformly distributed, suggesting that the reducing agents played a role in stabilizing the NPs. Figure 2 displays various FESEM-magnified images of (a) Ge, (b) AuNPs, (c) Ge/AuNPs and (d) Ge/PLA/AuNCs. The FESEM analysis demonstrated that the Ge/PLA/AuNCs exhibited oval-shaped structures. Moreover, in Fig. 2b, it was clearly seen that the AuNPs were spherical in size with an average particle size of 21 nm. Similar FESEM results have been reported for Au-NPs synthesized using plant extracts[43]. Among the different shapes observed for Ge/PLA/AuNCs, the spherical shape holds significant potential in the medical field. Its applications range from being a promising agent for anti-diabetic and anti-Alzheimer drugs to its spherical shape, which offers advantages in terms of drug delivery and targeted therapies[44]. However, due to the limited resolution of FESEM images, some obvious variations in the size and shape of Ge/PLA/AuNCs were observed.

HRTEM, DLS and Zeta potential analysis

The particle size confirmation of synthesized Ge/PLA/AuNCs was done using the hydrodynamic diameter analysis (Dynamic light scattering-DLS) and high-resolution transmission electron microscopy (HRTEM) analysis. HRTEM images reveal the synthesized Ge/PLA/AuNCs to be oval in shape, as shown in Fig. 3a. Figure 3a clearly shows that individual particle sizes ranged from 19 to 42 nm, and the average particle size was 21.57 nm. The hydrodynamic diameter was found to be 22 nm by DLS analysis (Fig. 3b), supporting the results obtained by HRTEM analysis. The particles were moderately stable in an aqueous solution possessing a zeta potential value of – 12.16 mV (Fig. 3c).

Swelling properties

This study examined the swelling properties of synthesized Ge, AuNPs, Ge/AuNPs and Ge/PLA/AuNCs over 5 min to 24 h, as shown in (Fig. S1a). We found that the swelling ratio varied for each synthesized sample. AuNPs had a swelling ratio of 35.42 ± 2.15%, Ge had a ratio of 58.37 ± 2.64%, Ge/AuNPs had a ratio of 70.19 ± 3.14%, and Ge/PLA/AuNCs had the highest swelling ratio of 90.48 ± 3.46%. These results indicate that Ge/PLA/AuNCs experienced a significant increase in their dimensions during the swelling process. Interestingly, after 20 and 24 h, we observed that Ge/PLA/AuNCs exceeded their weight limits, leading to the complete degradation of the nanocomposite biomaterial. The results suggest that Ge/PLA/AuNCs are highly prone to degradation under the given conditions. These findings are consistent with other research works with similar nanocomposites, further supporting the observed trends in swelling behavior and degradation[45]. The ability to control and predict the swelling behavior of these materials is crucial, as it enables researchers to tailor their characteristics to meet specific requirements.

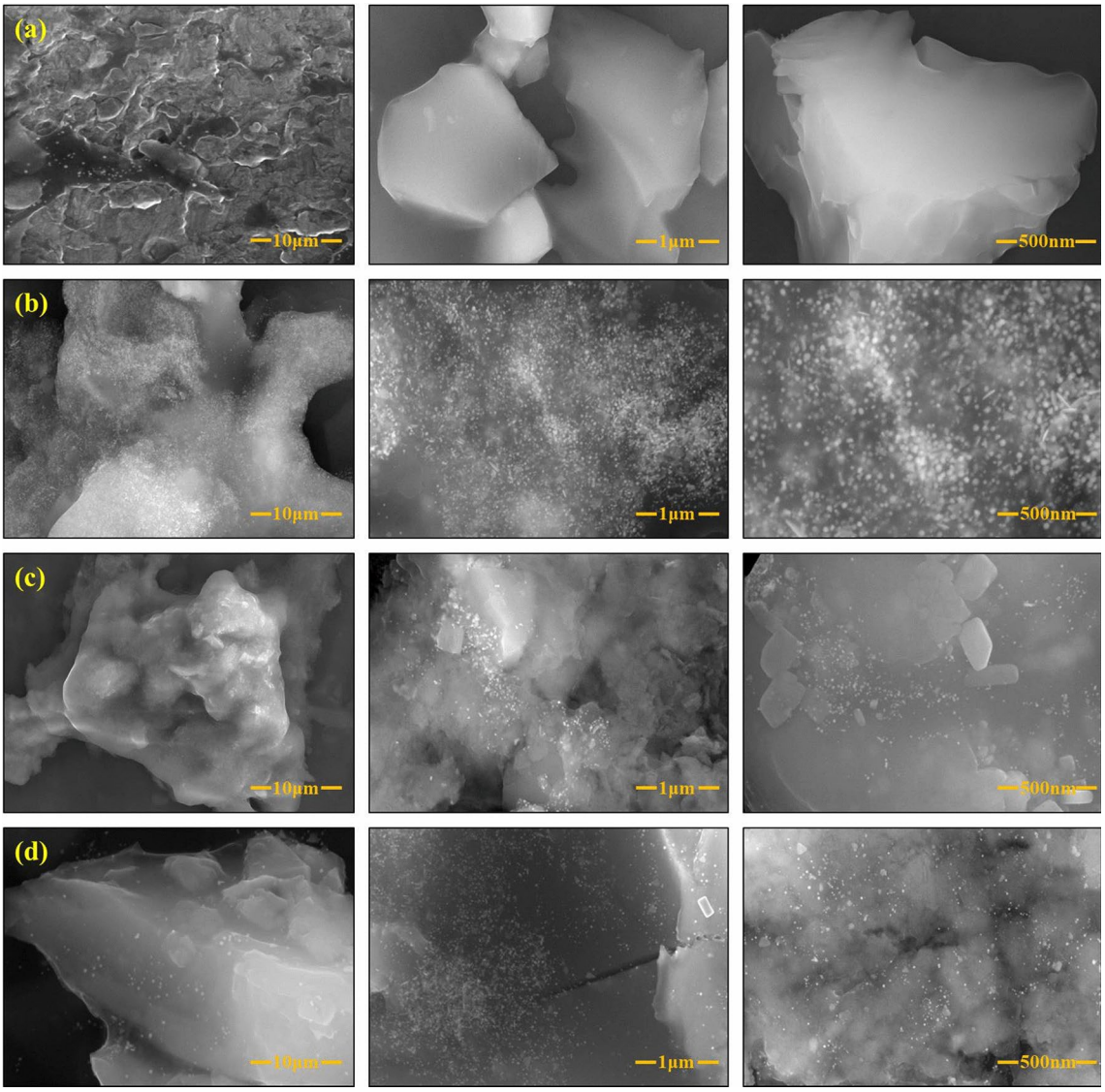

Fig. 2. FESEM morphology analysis of synthesized (**a**) gelatin, (**b**) AuNPs, (**c**) Ge/AuNPs and (**d**) Ge/PLA/AuNCs.

Cumulative drug release

In this study, we investigated the drug release properties of synthesized Ge, AuNPs, Ge/AuNPs and Ge/PLA/AuNCs, as depicted in (Fig. S1b). The Au release rate from Ge/PLA/AuNCs at various concentrations of 43.12 ± 2.48% for 0.5%, 60.38 ± 2.93% for 1%, 76.31 ± 3.12% for 1.5% and 90.46 ± 3.68% for 2%. The Ge/PLA/AuNCs demonstrated prolonged and controlled release properties of Au from Ge/PLA/AuNCs. The consistent results of this study align with prior reports that have investigated the drug-release properties of similar nanocomposites[46]. The remarkable swelling ratios exhibited by Ge/PLA/AuNCs further support their potential for controlled drug release applications. We selected Ge/PLA/AuNCs for further research in biomedical applications due to their outstanding swelling ratios and excellent controlled release properties. These findings open up exciting possibilities for developing novel drug delivery systems that can provide extended and controlled release of therapeutic agents, improving patient outcomes and treatment efficacy.

Antioxidant activity

Antioxidant activity is the power of antioxidant enzymes or compounds to remove or lessen the effects of reactive oxygen species (ROS), which lowers oxidative stress and keeps cells in balance. Moreover, researchers have carried out analytical determinations to identify and quantify secondary oxidation products. In our study, we used four distinct antioxidant studies to comprehensively understand the test samples' antioxidant capacity[47]. In our study, we used four distinct antioxidant studies to comprehensively understand the test samples' antioxidant capacity. These studies allowed us to evaluate the presence of primary and secondary oxidation products. By utilizing these antioxidant assays, we were able to gain valuable insights into the antioxidant capacity of the test samples. Environmental stress produces ROS, which can lead to the degradation of membrane lipids, proteins,

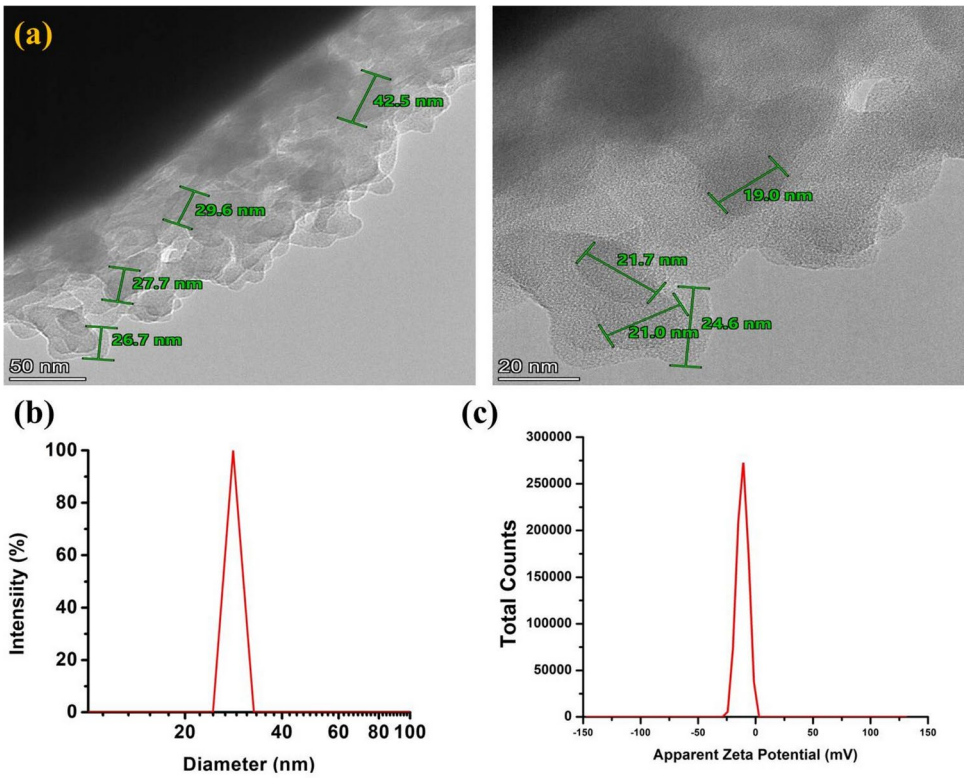

Fig. 3. The (**a**) TEM analysis, (**b**) DLS analysis and (**c**) Zeta potential analysis of synthesized Ge/PLA/AuNCs.

DNA, and plant cells. This, in turn, causes changes in plant metabolic pathways. This, in turn, causes changes in the plant metabolic pathways. In response to phenolics and oxidative stress, plants generate various metabolic substances, such as flavonoids and terpenoids[48,49]. To investigate the antioxidant capability of Ge/PLA/AuNCs generated by plants, we employed several in vitro antioxidant assays, including 2,2-Diphenyl-1-picrylhydrazyl (DPPH), 2,2′-azino-bis(3-ethylbenzothiazoline-6-sulfonic acid (ABTS), hydrogen peroxide (H_2O_2), superoxide dismutase (SOD), reducing power assays and Fluorescence recovery after photobleaching (FRAP).

In our study, at a concentration of 100 µg/mL, the Ge/PLA/AuNCs for DPPH scavenging activity were found to be 70.84 ± 1.64% (IC_{50} = 50.36 µg/mL), while the ABTS activity was 86.17 ± 1.96% (IC_{50} = 19.63 µg/mL). The H_2O_2 activity was measured at 60.74 ± 1.18% (IC_{50} = 68.35 µg/mL), SOD activity at 62.38 ± 1.26% (IC_{50} = 63.45 µg/mL), reducing power activity at 78.42 ± 1.48% (IC_{50} = 22.14 µg/mL) and FRAP activity at 61.73 ± 1.15% (IC_{50} = 64.07 µg/mL) as shown in Fig. 4. Notably, the ABTS reducing power activity and DPPH scavenging activity exhibited high levels of antioxidant activity, comparable to others. These findings highlight the strong antioxidant capacity of Ge/PLA/AuNCs generated by plants. The results of our study confirm that it has superior antioxidant properties compared to previous findings[47]. These Ge/PLA/AuNCs have an amazing ability to get rid of free radicals and have high antioxidant activity. This strongly supports their possible uses, especially in biomedical research.

In all of our experiments, we observed that the test samples exhibited improved dose-dependent antioxidant capability. In terms of ascorbic acid closer, the maximum antioxidant capacity was found to be for ABTS at a concentration of 100 mg/mL. Our study results showed that all test concentrations displayed outstanding free radical scavenging activity, as depicted in (Fig. 4a–f). These results show very close and excellent antioxidant activities compared to earlier reports that investigated different types of antioxidant properties of Mo-NiONPs[50]. The ability of the test samples to scavenge free radicals and exhibit high antioxidant activity is of enormous significance. Antioxidants play an important role in combating oxidative stress, which is linked to the development of many diseases[45]. Understanding these substances' antioxidant capabilities can contribute to the development of antioxidant-based therapies and materials that can protect against oxidative damage.

Antibacterial activity

In recent years, there has been an accelerated exploration of medicinal plants and plant-mediated nanomaterials for their potential antibacterial properties[44,51,52]. These natural sources offer a wide range of bioactive chemicals with well-established therapeutic characteristics[53]. The research aimed to assess the effectiveness of Ge/PLA/AuNCs against specific strains, including both gram-negative and gram-positive bacteria. The well-diffusion method entails placing the test sample inside a well in a confluent bacterial culture plate. The substance's diffusion from the well creates a concentration gradient, allowing for the assessment of its inhibitory effect on bacterial growth[54]. The zone of inhibition (ZOI), which restricts bacterial growth, offers valuable insights into the antibacterial activity of the tested substance.

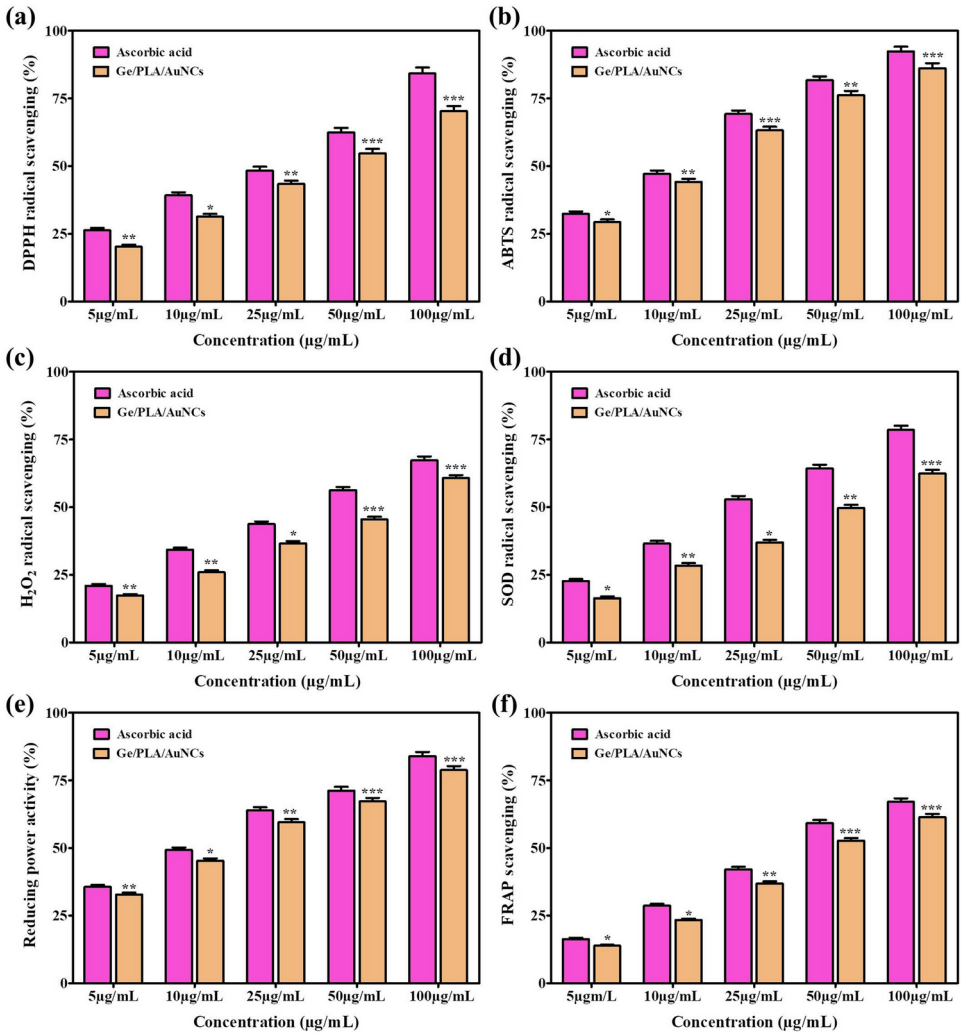

Fig. 4. Antioxidant activity of synthesized Ge/PLA/AuNCs for (**a**) DPPH, (**b**) ABTS, (**c**) H_2O_2, (**d**) SOD, (**e**) reducing power activity and (**f**) FRAP at various concentrations (5, 10, 25, 50 and 100 µg/mL). Values are expressed as mean ± SD (*$p < 0.05$; **$p < 0.001$; ***$p < 0.0001$). An asterisk indicates significant differences among treatments compared to control.

In our study, significant ZOI was observed in *Staphylococcus aureus* (19.45 ± 0.89 mm), *Bacillus subtilis* (18.51 ± 0.79 mm), *Enterococcus faecalis* (17.29 ± 0.81 mm) and *Micrococcus luteus* (18.93 ± 0.92 mm), as shown in Table 1. Moreover, significant zones of inhibition (ZOI) were observed for gram-negative bacteria, specifically *Escherichia coli* (20.83 ± 0.97 mm), *Klebsiella pneumoniae* (19.51 ± 0.90 mm), *Proteus vulgaris* (18.46 ± 0.83 mm), and *Salmonella typhi* (19.80 ± 0.89 mm), as illustrated in Table 1. Ge/PLA/AuNCs exhibited significant antibacterial efficacy, with a marked disparity in inhibition between Gram-negative and Gram-positive bacteria. At a dose of 100 µg/mL, Ge/PLA/AuNCs exhibited optimal bactericidal efficacy against all examined pathogenic bacterial strains, exceeding the positive control. Furthermore, the inhibitory activity of synthesized Ge/PLA/AuNCs demonstrated a robust dose-dependent relationship with pathogenic bacteria growth. Prior research has also highlighted the good antibacterial activity of hydrogel-AuNPs synthesized using *Chlorella vulgaris* plant extracts against various bacterial strains[55]. Researchers have reported that chitosan/poly(γ-glutamic acid)/AuNPs were investigated for antibacterial activity and showed excellent antibacterial activity[56]. A report suggests that AuNPs synthesized using *Euphorbia wallichii* extract have excellent antibacterial activity[57]. The assembly of polymer-AuNPs on the bacteria's membrane induces structural conformation changes and increased membrane permeability, ultimately resulting in bacterial cell death[58].

Anti-inflammatory activity

Inflammation is a natural response of the immune system to irritants, damaged cells, pathogens, and harmful stimuli[59]. However, the immune response can sometimes become exaggerated, leading to chronic inflammation. Researchers have found that certain metallic NPs and plant secondary metabolites have demonstrated anti-inflammatory activities[60]. AuNPs are used to protect flavonoids like isovitexin and hydroxycinnamic acid derivatives like chlorogenic acid, ferulic acid, and carboxylic acid. These compounds have shown potential for

Name of the pathogens	Zone of inhibition (mm) concentration (µg/mL)				
	PC	10	25	50	100
Gram-positive bacteria					
S. aureus	18.92 ± 0.97	12.04 ± 0.43*	14.56 ± 0.57***	16.38 ± 0.72**	19.45 ± 0.89***
B. subtilis	17.49 ± 0.85	10.48 ± 0.35**	12.71 ± 0.43**	15.46 ± 0.63*	18.51 ± 0.75***
E. faecalis	16.63 ± 0.76	10.97 ± 0.42*	12.04 ± 0.56**	14.83 ± 0.71***	17.29 ± 0.81**
M. luteus	17.82 ± 0.94	11.47 ± 0.48**	13.82 ± 0.61***	15.74 ± 0.79**	18.93 ± 0.92***
Gram-negative bacteria					
E. coli	19.52 ± 0.95	13.23 ± 0.49**	15.28 ± 0.62*	17.61 ± 0.81***	20.83 ± 0.97***
K. pneumonia	18.39 ± 0.84	12.61 ± 0.41**	14.60 ± 0.60***	16.92 ± 0.76**	19.51 ± 0.90**
P. vulgaris	17.04 ± 0.76	11.49 ± 0.36**	13.64 ± 0.52**	15.83 ± 0.69*	18.46 ± 0.83***
S. typhi	18.75 ± 0.89	12.98 ± 0.45*	14.75 ± 0.58***	16.53 ± 0.78**	19.80 ± 0.94**

Table 1. The antibacterial activity of synthesized Ge/PLA/AuNCs at different concentrations (10, 25, 50 and 100 µg/mL) against the gram-positive and gram-negative bacteria. The results are expressed as the mean ± SD. Statistical significance levels were indicated using asterisks, with *$p < 0.05$, **$p < 0.001$, and ***$p < 0.0001$ denoting different levels of significance.

Name of the drug	Conc. (µg/mL)	% inhibition			
		COX-1	IC_{50}	COX-2	IC_{50}
Ibuprofen	5	23.48 ± 0.47	42.28 µg/mL	27.15 ± 0.52	27.32 µg/mL
	10	34.67 ± 0.56		42.83 ± 0.68	
	25	47.19 ± 0.61		57.24 ± 0.79	
	50	60.82 ± 0.75		68.71 ± 0.89	
	100	72.45 ± 0.88		80.39 ± 0.96	
Ge/PLA/AuNCs	5	13.72 ± 0.32**	59.82 µg/mL	18.29 ± 0.39***	43.28 µg/mL
	10	26.49 ± 0.48**		30.74 ± 0.51*	
	25	40.18 ± 0.54*		49.52 ± 0.63**	
	50	52.79 ± 0.71***		62.95 ± 0.74**	
	100	64.28 ± 0.85***		74.84 ± 0.98***	

Table 2. Anti-inflammatory activity of Ge/PLA/AuNCs at different concentrations (5, 10, 25, 50 and 100 µg/mL) for COX-1 and COX-2. Ibuprofen was used as a positive control. The results are expressed as the mean ± SD. Statistical significance levels were indicated using asterisks, with *$p < 0.05$, **$p < 0.001$, and ***$p < 0.0001$ denoting different levels of significance.

reducing inflammation through various mechanisms. For example, they can inhibit COX, an enzyme producing prostaglandins and leukotrienes that contribute to inflammation. They can also have a differential action on COX-1 and COX-2, further reducing inflammation[61,62]. To test how well Ge/PLA/AuNCs work together to reduce inflammation activity, COX-1 and COX-2 in vitro mechanisms were used. The anti-inflammatory activity of these mechanisms was found to be excellent and was observed in both COX-1 (64.28 ± 0.85%) and COX-2 (73.84 ± 0.98%). The IC_{50} values were found to be 59.82 µg/mL for COX-1 and 43.28 µg/mL for COX-2, as shown in Table 2. The use of nanotechnology in medicine has opened up new possibilities for identifying and treating inflammatory and damaged areas in the body[63]. By utilizing nanocarriers like Ge/PLA/AuNCs, it is possible to enhance drug penetration into the active site of microbial infectious nanocarriers, thus improving the effectiveness of treatment.

Anti-diabetic activity

Diabetes mellitus is a metabolic disorder characterized by high levels of glucose in the blood, a condition known as hyperglycemia[64]. This condition is associated with various complications, including cardiovascular and neural disorders. Maintaining blood glucose levels within the normal range is crucial for managing diabetes and preventing these complications[64,65]. There are two important enzymes involved in carbohydrate metabolism: α-amylase and α-glucosidase. These enzymes play a crucial role in digestion by breaking down complex carbohydrates into simple glucose molecules. However, in diabetes, it is important to inhibit these carbohydrate digestive enzymes to control hyperglycemia[66]. Investigators have already established the anti-diabetic activity of many plant extracts[67], including *S. cumini* seed extracts[68]. By inhibiting these enzymes, this plant extract may help to regulate blood glucose levels and control hyperglycemia. In this study, Ge/PLA/AuNCs were bio-fabricated using *S. cumini* fruit extract, and their potential as an antioxidant-derived anti-diabetic agent was evaluated.

The results of our study showed that Ge/PLA/AuNCs, at the highest concentration of 100 µg/mL, exhibited significant anti-diabetic properties. The results showed that the 82.56 ± 1.49% of α-amylase and the 80.27 ± 1.57% of α-glucosidase had anti-diabetic activity (Fig. 5a,b). Additionally, IC_{50} values were calculated to be 27.86 µg/mL for α-amylase and 32.93 µg/mL for α-glucosidase. Ge/PLA/AuNCs effectively inhibit this enzyme, demonstrating their potential as anti-diabetic agents. A study using the *Curcuma longa* plant has shown that the mediated synthesis of nanoparticles has good inhibition activities of α-amylase (74.23 ± 0.42) and α-glucosidase (62.32 ± 0.48)[69]. The significant inhibition of α-amylase and α-glucosidase by Ge/PLA/AuNCs is attributable to the presence of phytochemicals, including flavonoids and polyphenols. The findings from the phytochemical study and FTIR corroborated this idea. These phytochemicals exhibit antioxidant effects that may mitigate oxidative damage. The results of phytochemical analysis and FTIR confirmed this hypothesis. These phytochemicals possess antioxidant properties, which can help reduce oxidative stress[47]. Moreover, by inhibiting the activity of carbohydrate hydrolyzing enzymes, Ge/PLA/AuNCs demonstrate their potential as effective anti-diabetic agents.

Anti-Alzheimer's activity

Alzheimer's disease is a prevalent and devastating neurodegenerative disease that typically leads to dementia and cognitive impairment, with symptoms generally worsening as individuals age[70]. The progression of the disease involves the hydrolysis of acetylcholine, an important neurotransmitter, by enzymes known as cholinesterases. In modern therapeutic approaches for the effective treatment of Alzheimer's disease, various synthetic and natural molecules have been explored to inhibit cholinesterase enzymes. These enzymes are known to play a significant role in the development and progression of Alzheimer's[70,71]. Researchers have identified several synthetic and natural compounds that effectively inhibit cholinesterase enzymes[72,73]. Nanotechnology, a vast field of research, offers potential opportunities for discovering new treatment techniques, particularly in drug delivery[36]. In this study, Ge/PLA/AuNCs were evaluated for their ability to inhibit AChE and BChE. Ge/PLA/AuNCs were evaluated in a concentration range of 5 µg/mL to 100 µg/mL.

Our study observed the inhibitory effects of Ge/PLA/AuNCs on AChE and BChE. The findings presented in Fig. 6 demonstrate that the inhibitory effect on both enzymes is contingent upon the dosage of Ge/PLA/AuNCs administered. The maximum inhibition values were recorded at a concentration of 100 µg/mL, showing 76.37 ± 1.18% inhibition for AChE and 85.94 ± 1.38% inhibition for BChE (Fig. 6a,b). The calculated IC_{50} values were 43.95 µg/mL for AChE and 32.63 µg/mL for BChE. Green synthesized AuNPs utilizing *Allium cepa* plant

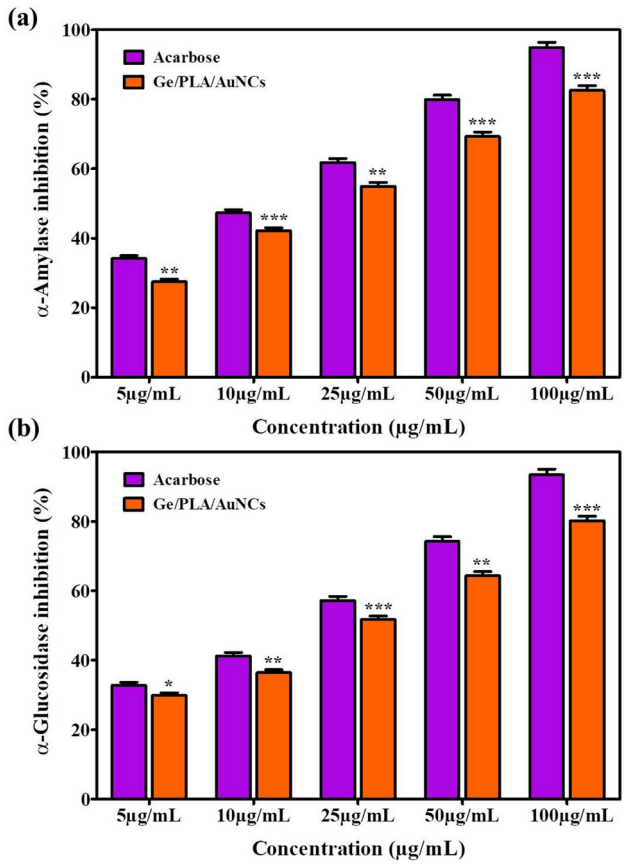

Fig. 5. Antidiabetic activity of synthesized Ge/PLA/AuNCs for (**a**) α-Amylase activity and (**b**) α-Glucosidase activity at various concentrations (5, 10, 25, 50 and 100 µg/mL). Values are expressed as mean ± SD (*$p < 0.05$; **$p < 0.001$; ***$p < 0.0001$). An asterisk indicates significant differences among treatments compared to control.

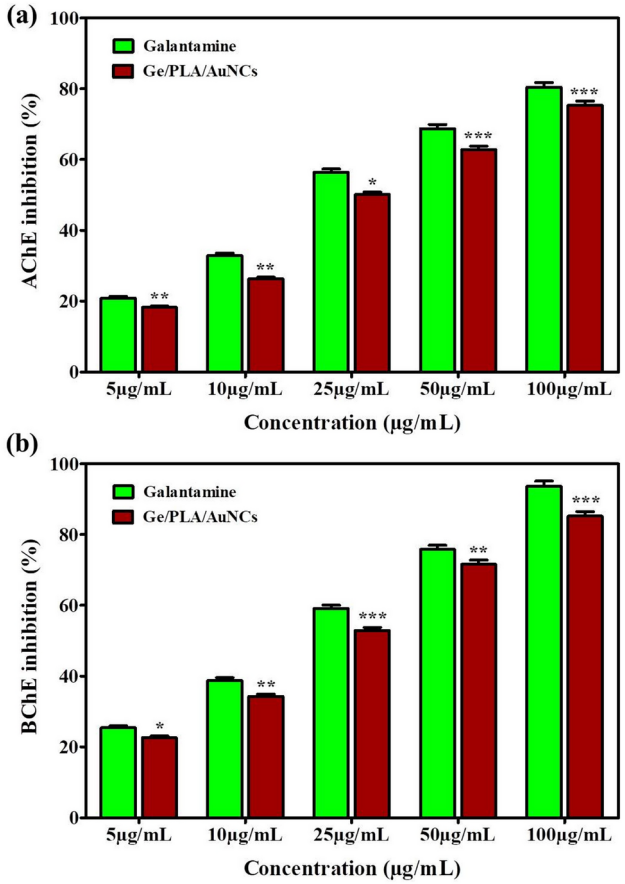

Fig. 6. Anti-Alzheimer's activity of synthesized Ge/PLA/AuNCs for (**a**) AChE activity and (**b**) BChE activity at various concentrations (5, 10, 25, 50, and 100 µg/mL). Values are expressed as mean ± SD (*$p < 0.05$; **$p < 0.001$; ***$p < 0.0001$). An asterisk indicates significant differences among treatments compared to control.

extract demonstrated notable inhibitory effects on AChE and BChE enzymes during the assessment of anti-cholinesterase activities[74]. Another study demonstrated that biogenic AuNPs inhibited AChE and BChE by 81% and 85%, respectively[75]. The findings of our study demonstrate the potential of Ge/PLA/AuNCs as elements for targeted delivery in prospective Alzheimer's treatments. The observed inhibitory effects on AChE and BChE, coupled with the dosage-dependent response, indicate that Ge/PLA/AuNCs may hold potential for applications in the management and treatment of Alzheimer's disease. Metal ions are recognized for their significant role in the degradation of amyloids both in the brain and in vitro[76]. Brain autopsies of Alzheimer's patients exhibit a higher concentration of aluminium, zinc and copper compared to normal brains. Moreover, zinc has been found to elicit amorphous aggregates in Aβ compared to fibrillar structure induced by iron[77]. On the other hand, gold nanoparticles have demonstrated that they can dissociate amyloid aggregates in vitro[78,79]. Thus, our synthesized nanocomposite, loaded with Au nanoparticles, can elicit anti-amyloid activity by interfering with the amyloid-forming enzymes, resulting in reduced amyloid formation.

In vivo biocompatibility assay

The transparent zebrafish embryos were used as a model to evaluate the biocompatibility and toxicity of the Ge/PLA/AuNCs. Observations were made at 6 h post-fertilization (hpf), 30 hpf, 54 hpf, 72 hpf, 78 hpf, 90 hpf, and 114 hpf for untreated control groups and groups treated with the extract at 100 µg/mL and 200 µg/mL. The number of hatched embryos was recorded, and any developmental abnormalities were examined under a light microscope. Typical images of embryos before hatching (at 6 hpf, 30 hpf, 54 hpf, 72 hpf, and 90 hpf) are shown in (Fig. 7a). The results indicated no abnormalities following treatment with the Ge/PLA/AuNCs at 100 µg/mL. However, a tail bent was observed at a high dose (200 µg/mL), and incomplete hatching was also seen. The hatchability at the higher dose was 75%, which is within acceptable toxicity limits. Ge/PLA/AuNCs are safe, as shown by the fact that there was no significant difference in the cumulative hatchability of embryos treated with 100 µg/mL compared to the control group that wasn't treated (Fig. 7b).

Cell viability assay

Zebrafish embryos showed no abnormalities or toxicity after treatment with Ge/PLA/AuNCs, which shows that Ge/PLA/AuNCs are non-toxic up to a dose of 100 µg/mL. Therefore, Ge/PLA/AuNCs were directly investigated for neuron production activity. Further study was conducted to evaluate the impact of Ge/PLA/AuNCs on cell

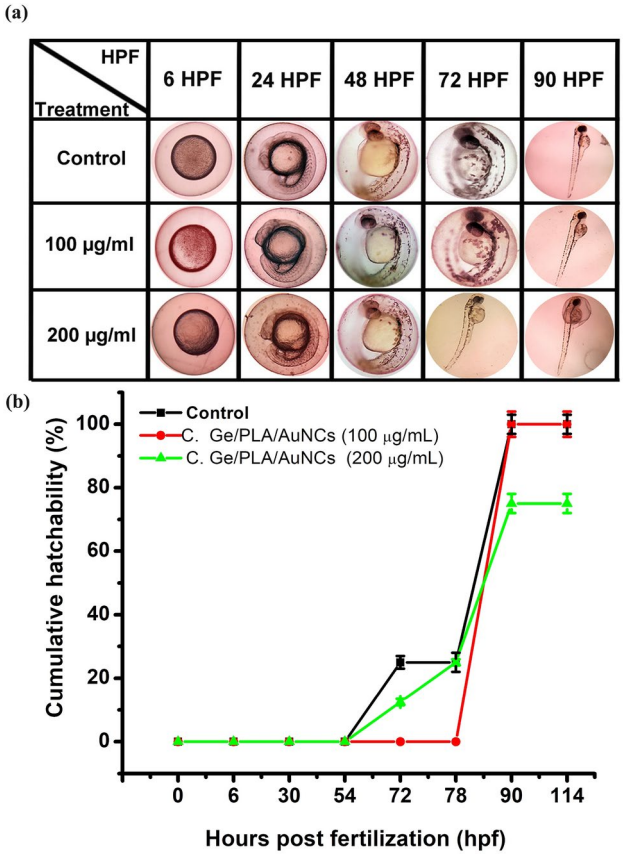

Fig. 7. (**a**) The microscopic images and (**b**) the cumulative hatchability of zebrafish embryos for untreated and treated (Ge/PLA/AuNCs (100 µg/mL and 200 µg/mL) groups after different hours post fertilization (hpf).

viability and neurotoxicity using the human neuroblastoma cell line SH-SY5Y. As depicted in (Fig. 8a), our study results demonstrated a dose-dependent improvement in cell viability with increasing concentrations of Ge/PLA/AuNCs compared to high glucose (Hg) treatment. In the study, high-glucose-treated cells exhibited a significant reduction in cell viability of 20.18 ± 0.82% compared to the control. Conversely, SH-SY5Y cells treated with Ge/PLA/AuNCs at different concentrations showed enhanced cell viability. At the highest concentration of 100 µg/mL, cell viability reached 95.27 ± 1.62% compared to the high glucose-treated cells. These findings suggest that higher concentrations of Ge/PLA/AuNCs positively impact maintaining cell viability.

The results of the microscopic examination, as presented in (Fig. 8b) are consistent with the cell viability findings, and the neuronal cells are found to be spherical in shape and well-proliferated compared to the control[80]. SH-SY5Y cells treated with Ge/PLA/AuNCs displayed reduced neuronal damage and increased neuronal growth factors compared to the high glucose-treated and control cell lines. This indicates that the highest concentration (100 µg/mL) of Ge/PLA/AuNCs evaluated in the study positively reduced the neurotoxic effects induced by high glucose. In comparison to earlier reports, the synthesis of AuNPs with plant extracts and the SH-SY5Y cell viability assay yielded similar results[81]. These findings suggest that using Ge/PLA/AuNCs and assessing cell viability using the SH-SY5Y cell line provide consistent findings and support the potential of Ge/PLA/AuNCs in various biomedical applications.

Materials and methods

Materials

Gold(III) chloride ($HAuCl_4$), gelatin (Types-A), PLA, glycerol, DPPH, ABTS, Ethylenediaminetetraacetic Acid (EDTA), riboflavin, specific inhibitors for COX-1 (FR122047-KT) and COX-2 (FK3311-KT), 4-nitrophenyl-α-D-maltopentaoside, 4-nitrophenyl-D-glucopyranoside, Acetylthiocholine iodide (AChI)/butyrylcholine iodide (BChI) were purchased from Sigma-Aldrich, India. Hydrogen peroxide, ascorbic acid, NBT (Nitroblue Tetrazoliumtrichloroacetic acid), sodium phosphate, potassium ferricyanide, Mueller-agar, α-amylase were purchased from Himedia, India. Gram-positive (*Staphylococcus aureus, Bacillus subtilis, Enterococcus faecalis* and *Micrococcus luteus*) and Gram-negative (*Escherichia coli, Klebsiella pneumoniae, Proteus vulgaris,* and *Salmonella typhi*) strains were obtained from NCIM, Pune, India. SH-SY5Y neuroblastoma cell line was procured from NCBI, Pune, India. Zebrafish was obtained from Tarun Fish Farm, Kelambakkam, Chennai.

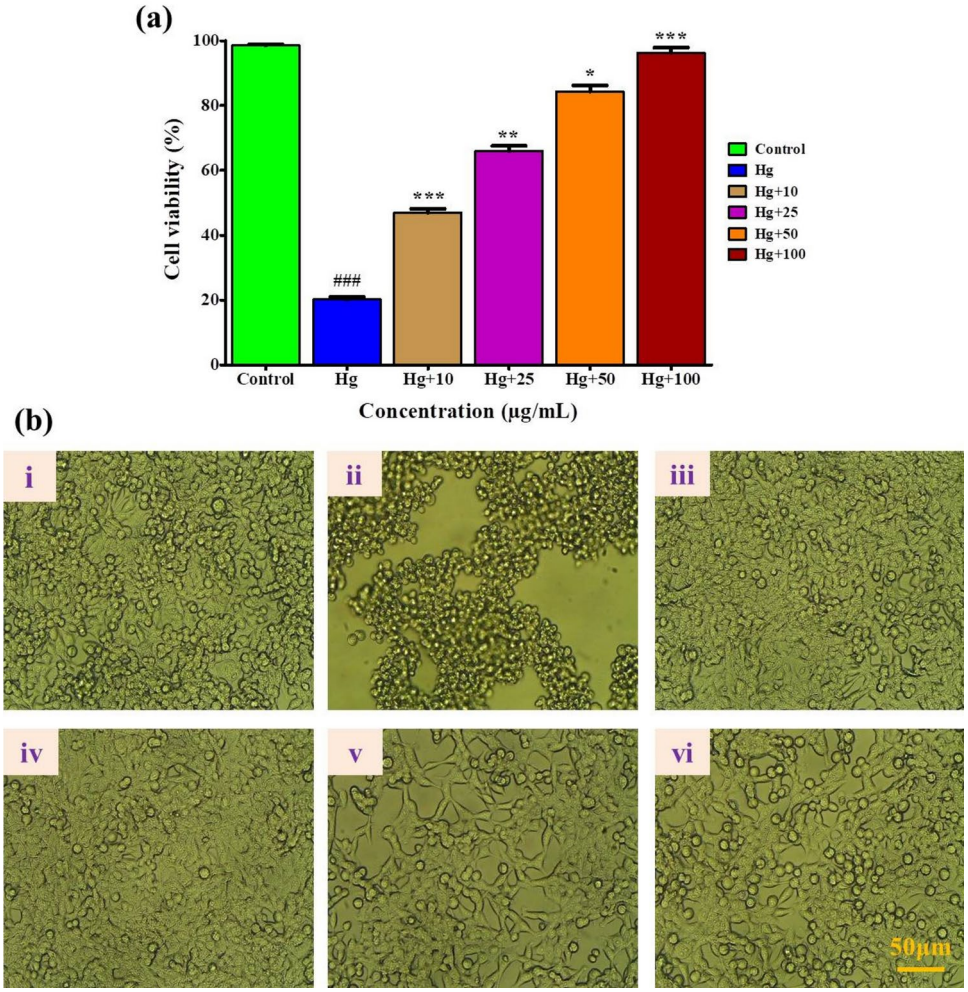

Fig. 8. (**a**) Cell viability assay of synthesized Ge/PLA/AuNCs for SH-SY5Y cell lines and (**b**) microscopic study i) control, ii) high glucose (Hg), iii) 10 µg/mL, iv) 25 µg/mL, v) 50 µg/mL and vi) 100 µg/mL. Scale bar: 50 µm. The values are expressed as mean ± SD. The significance levels were indicated by asterisks (*$p < 0.05$, **$p < 0.001$ and ***$p < 0.0001$).

Preparation of *Syzygium cumini* plant extract

The *S. cumini* fruits were obtained from a medicinal plant garden located at SSN College Campus in Chennai. The harvested fruits were subjected to an extensive cleaning procedure using distilled water to guarantee cleanliness. Thereafter, the fruits were diced into small segments to extract the pulp. Five grammes of the fruit were combined with 100 ml of distilled water. The resultant mixture was further heated to 50 °C for 60 min. An extensive filtration method was utilized to guarantee the extract's purity. The extract was initially filtered twice through nylon paper to eliminate bigger contaminants. The extract was subjected to three filtration cycles utilizing Whatman No. 1 filter paper. To ensure its freshness and keep its qualities, the extract was subsequently stored in a refrigerator at a temperature of 4 °C[31].

Synthesis of AuNPs

A slightly modified version of an established method was used to synthesize AuNPs[18,19]. Briefly, 90 mL of 1 mM $HAuCl_4$ and 10 mL of the *S. cumini* plant fruit extract was combined in a ratio of 9:1. The mixture was maintained at 60 °C for 3 h under magnetic stirrer conditions. The efficacious synthesis of AuNPs was validated by the distinct color transformation of the solution, shifting from a pale-yellow hue to a vibrant ruby-red shade. The mixture underwent centrifugation at 10,000 rpm for 30 min. This process enabled the separation of a pellet, followed by three rounds of sterile water washing to eliminate any remaining impurities. Finally, the resulting solution was dried and pulverized, preparing it for further investigation and analysis.

Nanofabrication of Ge/PLA/AuNCs

The synthesis of the nanocomposite was done with minor changes utilizing a previously reported method[19,35,82]. Initially, gelatin (G9391-100G, Sigma, India) was solubilized in phosphate-buffered saline (PBS) at a concentration of 2%, while PLA (GF45989881-1EA, Sigma, India) was separately dissolved in ethyl acetate at a concentration of 2%, both under stirring for 3 h at 500 rpm to achieve complete dissolution. Subsequently, in a conical flask,

80 mL of AuNPs solution, 10 mL of gelatin, and 10 mL of PLA were amalgamated in a ratio of 8:1:1. The solution was subsequently positioned on a magnetic stirrer and maintained at 60 °C for duration of 6 h. To improve flexibility, 5 mL of a 1% glutaraldehyde solution, a cross-linking agent, was included. Furthermore, 500 µL of glycerol was included as a plasticizer in the polymer blends. The heterogeneous solution was agitated at 60 °C for 3 h to facilitate the reaction. Subsequent to the reaction, the mixture underwent centrifugation at 12,000 rpm. The resultant precipitate was subsequently dried and pulverized use a lyophilizer. The nanocomposite was meticulously collected and subsequently transferred to a sealed glass vial for storage. The solution's stability was preserved by keeping it at − 20 °C for future use.

Characterization of Ge/PLA/AuNCs

The synthesized Ge/PLA/AuNCs were analyzed employing several spectroscopic techniques. The Ge/PLA/AuNCs were predominantly analyzed via UV–Vis spectroscopy. The Shimadzu UV-1800 instrument was employed to assess the absorption of the nanocomposites across the wavelength spectrum of 200 to 800 nm. Fourier transform infrared spectroscopy (FTIR) was utilized to elucidate the functional groups of the nanocomposites. The study was conducted utilizing a Perkin Elmer machine with a range of 400 to 4000 cm^{-1}. A potassium bromide (KBr) pellet-FTIR-grade technique was employed, and X-ray diffraction analysis was performed to investigate the crystalline characteristics of the Ge/PLA/AuNCs. An XRD-X'Pert Pro device manufactured in the USA was utilized for this objective. FESEM (Thermo Fisher Scientific, Apreo 2 s HiVac, USA) was utilized to precisely evaluate the dimensional and morphological attributes of the Ge/PLA/AuNCs. The data acquired from the FESEM images was subsequently analyzed via IMAGE J software. The hydrodynamic diameter and zeta potential were assessed via the Malvern Zeta Sizer[83]. The material was dissolved in distilled water and sonicated in a water bath for five minutes prior to analysis. High-Resolution Transmission Electron Microscopy (HRTEM) examination was conducted utilizing a Thermo Fisher Scientific apparatus, USA, operating at 80 Hz, to determine the dimensions of the nanocomposite[84].

Swelling properties

An experiment was performed to investigate the swelling characteristics of Ge, AuNPs, Ge/AuNPs, and Ge/PLA/AuNCs composites[85]. The samples were solubilized in PBS and continuously monitored at 37 °C for 24 h. Upon the completion of the specified duration, the solution underwent a swelling assessment. Samples were collected from the PBS solution at predetermined intervals for subsequent analysis. To guarantee precise measurements, any surface moisture on the samples was meticulously eliminated using tissue paper. After the elimination of surface droplets, the samples were weighed. The swelling ratio of the samples was then calculated using the following "Eq. (1)":

$$\text{Swelling ratio}\,(\%) = \frac{W_t - W_0}{W_0} \times 100 \tag{1}$$

In this formula, W_t represents the swollen sample weight at a specific time point, while W_0 denotes the initial weight of the sample before the swelling experiment.

In vitro drug release study

The dialysis membrane diffusion technique was utilized to examine the in vitro release properties of synthesized Ge, AuNPs, Ge/AuNPs, and Ge/PLA/AuNCs[86]. A specimen of Ge, AuNPs, Ge/AuNPs, and Ge/PLA/AuNCs was placed into separate dialysis bags. Each dialysis bag carrying the corresponding sample was immersed in a beaker. The beaker contained 100 mL of PBS (pH 7.4) with 0.5% Tween 80. The system was kept at a stable temperature of 37 ± 2 °C. The system was agitated at a velocity of 100 rpm to guarantee homogeneous mixing and promote release. Samples were extracted from the external release media surrounding the dialysis bag at predetermined time intervals. The volume of the collected medium was promptly substituted with an equivalent volume (0.5 mL) of PBS to preserve sink conditions. The concentrations of Ge, AuNPs, Ge/AuNPs, and Ge/PLA/AuNCs in the obtained samples were quantified. A UV–Vis spectrophotometer was employed for these observations, precisely at a wavelength (λ) of 446 nm. The entire experiment was conducted in triplicate to ensure accuracy and reliability.

In-vitro antioxidant assays of Ge/PLA/AuNCs

DPPH assay

The DPPH assay was performed following a described known method[87]. A 4 mL solution of 0.2 mM DPPH was mixed with Ge/PLA/AuNCs at different concentrations (5, 10, 25, 50, and 100 µg/mL). The mixture was equilibrated at room temperature (25 °C) for 30 min in dark. During the reaction, the solution color changed from purple to yellow, indicating the reduction of the DPPH radical by the Ge/PLA/AuNCs. Absorbance data were obtained using a UV–vis spectrophotometer at 517 nm, and the positive control used for the study was ascorbic. DPPH radical scavenging activity was estimated using the following equation "Eq. (2)":

$$\text{Inhibition}\ (\%) = \left[\frac{\text{Absorbance}\ (\text{Control}) - \text{Absorbance}\,(\text{Sample})}{\text{Absorbance}\ (\text{Control})}\right] \times 100 \tag{2}$$

ABTS assay

The ABTS radical ($ABTS^{\cdot+}$) activity assay was performed following a recognised protocol[88]. 5 mL of a 7 mM ABTS solution in distilled water was prepared to commence the experiment. Subsequently, 88 µL of a 140 mM potassium persulfate ($K_2S_2O_8$) solution was incorporated into the ABTS solution. The combination was incubated

at room temperature for 12 to 16 h, facilitating the production of a blue ABTS solution. The antioxidant activity of the sample was assessed using the solutions outlined below. The test tubes were made by combining the ABTS solution with Ge/PLA/AuNCs at various concentrations (5, 10, 25, 50, and 100 µg/mL). Each tube was permitted to remain at room temperature for 10 min in a dark environment to facilitate the reaction. Following incubation, the absorbance of each sample was assessed at λ = 734 nm, with ascorbic acid serving as the positive control in this test. The ABTS· + value was determined using the previously referenced Eq. (2).

Hydrogen peroxide (H_2O_2) radical scavenging assay
The H_2O_2 assay was performed following an established method known earlier[89]. The assay mixture consisted of H_2O_2 solution (6 mM), $FeSO_4$ solution (1.5 mM), and sodium salicylate solution (20 mM), with a total volume of 3 mL. Subsequent to a 5-min interval, varying amounts (5, 10, 25, 50, and 100 µg/mL) of Ge/PLA/AuNCs were introduced to the mixture. The resultant solution was incubated undisturbed for 30 min at 37 °C to facilitate the scavenging reaction. The resulting solution was incubated undisturbed for 30 min at 37 °C to allow the scavenging reaction to occur. Following the incubation period, the absorbance of the sample was measured using a UV–vis spectrophotometer set at a wavelength (λ) of 562 nm. Ascorbic acid was used as the positive control in the experiment. The $H_2O_2^{\cdot+}$ value was calculated using Eq. (2), as mentioned earlier.

Superoxide dismutase (SOD) activity
The ability of Ge/PLA/AuNCs to scavenge superoxide radicals was evaluated using a method established before[90]. To prepare the reaction mixture, 1 mM of EDTA, 50 mM of PBS, and 0.02 mM of riboflavin were added. Subsequently, 0.75 mM NBT (Nitroblue Tetrazolium) was added to the mixture. Different concentrations of Ge/PLA/AuNCs (5, 10, 25, 50, and 100 µg/mL) were included in the reaction mixture. The reaction mixture containing Ge/PLA/AuNCs, was exposed to fluorescent lamb for 7 min. After the light exposure, the scavenging activity of the Ge/PLA/AuNCs was measured at a wavelength (λ) of 560 nm using a spectrophotometer. Ascorbic acid was used as the positive control in the assay. The superoxide dismutase (SOD) activity of Ge/PLA/AuNCs was calculated using Eq. (2), as mentioned earlier.

Reducing power (RA) assay
The decreasing capability of Ge/PLA/AuNCs was examined according to the previously described procedure[91]. Various quantities of Ge/PLA/AuNCs (5, 10, 25, 50, and 100 µg/mL) were incorporated into a solution containing 200 mM sodium phosphate buffer and ferricyanide. The mixture was incubated at 50 °C for 20 min. To terminate the reaction and stabilise the mixture, 50 µL of trichloroacetic acid (TCA) was introduced. The reaction mixture was subjected to centrifugation at 3000 rpm for 10 min. Additionally, 50 µL of the supernatant was introduced to microtiter plates in conjunction with 0.1% ferric chloride. The microtiter plates underwent an additional incubation period of 10 min. Following the incubation period, the absorbance of the samples on the microtiter plates was quantified at a designated wavelength (λ) of 700 nm utilising a spectrophotometer. Ascorbic acid served as the positive control. The reduction capability of the Ge/PLA/AuNCs was determined using Eq. (2) as previously stated.

Ferric reducing antioxidant power (FRAP) assay
The diminishing efficacy of Ge/PLA/AuNCs was assessed following the previously outlined methodology[92]. Different concentrations of Ge/PLA/AuNCs (5, 10, 25, 50, and 100 µg/mL) were integrated into a solution including 200 mM sodium phosphate buffer and ferricyanide. The amalgamation was incubated at 50 °C for 20 min. To halt the reaction and stabilise the mixture, 50 µL of trichloroacetic acid (TCA) was added. The reaction mixture underwent centrifugation at 3000 rpm for 10 min. Furthermore, 50 µL of the supernatant was added to microtiter plates together with 0.1% ferric chloride. The microtiter plates experienced a supplementary incubation duration of 10 min. Subsequent to the incubation period, the absorbance of the samples on the microtiter plates was measured at a specified wavelength (λ) of 700 nm using a spectrophotometer. Ascorbic acid functioned as the positive control. The reduction capacity of the Ge/PLA/AuNCs was assessed utilising Eq. (2) as previously mentioned.

Antibacterial activity of Ge/PLA/AuNCs

The antibacterial efficacy of Ge/PLA/AuNCs was assessed via the agar well diffusion method against Gram-positive (*Staphylococcus aureus, Bacillus subtilis, Enterococcus faecalis,* and *Micrococcus luteus*) and Gram-negative (*Escherichia coli, Klebsiella pneumoniae, Proteus vulgaris,* and *Salmonella typhi*) strains sourced from NCIM, Pune, India[93]. Each bacterial culture utilised in this study was individually sustained in 5 mL of nutritional broth (NB) for 24 h at 37 °C. Each bacterial strain was thereafter injected onto the surface of Mueller–Hinton agar plates using a swab. Different concentrations of Ge/PLA/AuNCs (5,10, 25, 50, and 100 µg/mL) were poured into wells preformed on agar plates, which were incubated for 24 h at 37 °C. Following the experimental procedure, the clear zone of inhibition diameter (ZI) surrounding each well was measured in millimeters (mm). To establish a reference point for comparison, the broad-spectrum antibiotic streptomycin was used as the positive control.

Anti-inflammatory activity

To thoroughly evaluate the anti-inflammatory activity of Ge/PLA/AuNCs, the activities of both cyclooxygenase-1 (COX-1) and cyclooxygenase-2 (COX-2) enzymes were measured[94]. To assess these inhibitory activities, specific inhibitors for COX-1 (FR122047-KT, Sigma, India) and COX-2 (V FK3311-KT, Sigma, India) were utilized. As for the substrate selection, arachidonic acid was employed at a concentration of 1.1 mM. According to the instructions provided in the manufacturer's kit, the COX peroxidase constituents were calculated. This study chose a concentration of 10 mM ibuprofen as the positive control. A 96-well microplate was used to conduct

the analysis, with N,N,N′,N′-tetramethyl-p-phenylene diamine being examined. The plate reading was recorded using a Synergy II reader for 5 min at a wavelength of 590 nm.

Anti-diabetic enzyme inhibition assay

α-Amylase inhibition assay

The ability of Ge/PLA/AuNCs to inhibit α-amylase was evaluated using a chromogenic method[95]. In PBS (0.1 M, pH 6.8), the α-amylase enzyme was prepared at a concentration of 1 µg/mL. A 4-nitrophenyl-α-D-maltopentaoside solution (5 mM) was thoroughly mixed with the enzyme solution. To facilitate the enzymatic reaction, the enzyme and substrate mixture were incubated at a temperature of 37 °C for 30 min. After incubation, a small sample volume was added to the reaction mixture containing Ge/PLA/AuNCs (5,10, 25, 50 and 100 µg/mL). The sample activity was calculated as percent inhibition by calculating the difference in absorbance in the presence and absence of Ge/PLA/AuNCs in the reaction mixture. A microplate reader set to 405 nm was used to measure the absorbance. α-amylase (%) was estimated using the following equation:

$$\alpha - \text{amylase inhibition } (\%) = \left[\frac{\text{Absorbance (Control)} - \text{Absorbance (Sample)}}{\text{Absorbance (Control)}}\right] \times 100$$

a-glycosidase inhibition assay

An experiment was conducted to evaluate the potential of the test sample as an anti-diabetic agent[95]. The experiment aimed to assess the inhibition of α-glycosidase using a chromogenic technique. This technique involved the utilization of a polyethylene filter (0.45 µm) end-capped column. A small volume of the test sample was taken and mixed with Ge/PLA/AuNCs (5,10, 25, 50, and 100 µg/mL) and 5 mM of 4-nitrophenyl-D-glucopyranoside. The mixture was then incubated at 37 °C for 30 min. The optical density of the mixture was measured at a wavelength of 405 nm, both with and without the test materials, to assess their activity. The percent inhibition, reflecting the sample's activity, was determined by subtracting the absorbance values with and without samples from the absorbance of the tested sample. α-glycosidase (%) was calculated using the following equation:

$$\alpha - \text{glucosidase inhibition } (\%) = \left[\frac{\text{Absorbance (Control)} - \text{Absorbance (Sample)}}{\text{Absorbance (Control)}}\right] \times 100$$

Anti-cholinesterase enzyme inhibition assay

The in-vitro effects of the Ge/PLA/AuNCs on AChE and BuChE from electric eel (*Electrophorus electricus)* serum and equine serum, respectively, was assessed according to the Ellman's method as followed earlier[96,97]. To prepare the analogues for experimentation, they were solubilized in DMSO at a concentration of 1 mg/mL. The final reaction mixture contained 1% of DMSO. The substrates for the enzymatic reaction were Acetylthiocholine iodide (AChI)/butyrylcholine iodide (BChI) (Sigma-Aldrich, Saint Louis, MO, USA). To conduct this assay, 100 µL of Tris/HCl buffer (pH 8.0, 1.0 M) and different concentrations of the Ge/PLA/AuNCs (5, 10, 25, 50, and 100 µg/mL) were added to 50 µL of AChE/BuChE solution (5.32×10^{-3} µg/mL). The components were mixed properly, and the mixture was incubated 10 min at 20 °C. Then, to initiate the enzyme reaction, 50 µL of 5,5′-dithio-bis 2-nitro-benzoic acid (DTNB aka Ellman's reagent, 0.5 mM, Sigma-Aldrich, Saint Louis, MO, USA) and the substrates, AChI/BChI were added and incubated for a period of time. Then, the activities of AChE/BChE were determined spectrophotometrically by measuring the absorbance at $\lambda = 412$ nm. The calculation of AChE/BChE (%) was done using the following equation:

$$V = \Delta Abs/\Delta t$$

$$\text{Enzyme activity } (\%) = V/V \text{ maximum} \times 100$$

$$\text{Enzyme inhibition } (\%) = 100 - \text{enzyme activity } (\%)$$

In vivo biocompatibility assay using zebrafish embryos

Any engineered nanoparticles can be safely used to treat various diseases if they are biocompatible. Due to their transparent nature, zebrafish embryos are a popular model for conducting in vivo studies[98,99]. All developmental stages of these transparent embryos can be monitored under a light microscope, allowing for the identification of abnormalities such as tail bends and pericardial edema. The biocompatibility of the synthesized Ge/PLA/AuNCs at concentrations of 100 µg/mL and 200 µg/mL was assessed using zebrafish embryos, following ethical clearance from the Institutional Animal Ethics Committee of Chettinad Academy of Research and Education, Kelambakkam (IAEC2/Proposal: 162/A.Lr: 124/Dt: 02.07.2024). All methods were performed in compliance with the pertinent guidelines and regulations established by the Committee for Control and Supervision of Experiments with Animals (CCSEA), India. The study is conducted in compliance with ARRIVE criteria. Untreated embryos functioned as the control group, and standard pictures were obtained at 40X magnification. In each group, 10 embryos were preserved in duplicates. The cumulative hatchability was calculated using the equation provided below[98]:

$$\text{Cumulative hatchability } (\%) = \left[\frac{\text{Number of eggs hatched}}{\text{Initial number of eggs taken for treatment}}\right] \text{x } 100$$

Cell viability assay

The cell viability of Ge/PLA/AuNCs was assessed using SH-SY5Y neuroblastoma cell lines (NCBI, Pune, India). The SH-SY5Y cells were maintained in Dulbecco's Modified Eagle's Medium (DMEM) supplemented with 10% fetal bovine serum (FBS). To initiate the cell culture, 100 µL of SH-SY5Y cells, with a density of 1.9×10^{-5} cells/well, were added to each well of a 96-well plate. The plate was thereafter incubated overnight at 37 °C in a humidified chamber with a 5% CO_2 environment to facilitate cell adhesion and proliferation. Sequential dilutions of Ge/PLA/AuNCs were formulated at concentrations of 10, 25, 50, and 100 µg/mL. The diluted nanocomposites were introduced into each well of the plate containing SH-SY5Y cells. The dish was subsequently incubated for 24 h to facilitate the interaction between the cells and the nanocomposites. Following incubation, 10 µL of WST (Water-Soluble Tetrazolium) reagent was introduced to each well. The dish was subsequently incubated for a further four hours. The absorbance of the WST formazan product, indicative of cell viability, was quantified at a wavelength of 570 nm utilizing a spectrophotometer. The cell viability % was determined using absorbance measurements. The experiments were conducted thrice to guarantee precision and dependability. Confocal microscopy (CLSM-Nikon, TE2000, US) was used to capture microscopic images of the treated SH-SY5Y cell line for further analysis[100].

$$\text{Cell viability } (\%) = \left[\frac{\text{Absorbance of treated cells}}{\text{Absorbance of control}}\right] \text{x } 100$$

Statistical analysis

The characterization analysis was conducted using Origin Pro software (Origin Pro-2024). To perform the statistical analyses, GraphPad Prism software was utilized (GraphPad Prism, version 5). For the statistical analysis, a one-way analysis of variance (ANOVA) followed by Tukey's multiple comparisons was employed to determine the significance values. The results of the analysis were presented as the mean ± standard deviation (mean ± SD). In all probability tests conducted during the study, a significance level of $p < 0.05$ was employed to determine the presence of significant differences.

Conclusions

In conclusion, this study describes the biosynthesis of Ge/PLA/AuNCs using *S. cumini* fruit extract and its possible various biomedical applications. The synthesized Ge/PLA/AuNCs were confirmed at 534 nm through UV–vis spectrum analysis. FTIR analysis confirmed the presence of various functional groups, while XRD analysis confirmed the crystalline structure of the synthesized Ge/PLA/AuNCs. Additionally, FESEM analysis revealed the spherical shape of the Ge/PLA/AuNCs, and the HRTEM image showed the spherical in shape and the average size range of 21 nm. The Ge/PLA/AuNCs exhibited promising antioxidant activities. The synthesized Ge/PLA/AuNCs exhibited impressive antibacterial activity against both Gram-positive and Gram-negative bacteria. The Ge/PLA/AuNCs showed efficient anti-inflammatory properties by inhibiting the COX-1 (64.28%) and COX-2 (73.84%) enzymes. The study revealed that Ge/PLA/AuNCs had a moderate inhibitory effect on α-amylase (82.56%) and α-glucosidase (80.27%) enzymes. Ge/PLA/AuNCs have effective anti-Alzheimer activity because they inhibited both AChE (76.37%) and BChE (85.94%) enzymes. The Ge/PLA/AuNCs also exhibited excellent in vivo biocompatibility up to a dose of 100 µg/mL in zebrafish embryos. In the SH-SY5Y cell lines, the Ge/PLA/AuNCs demonstrated improved cell viability and enhanced neuronal cell growth. Overall, this study underlines that Ge/PLA/AuNCs have excellent antioxidant, antibacterial and diverse biomedical applications.

Data availability

The datasets used and/or analyzed during the current study are available from the corresponding author upon reasonable request.

Received: 12 August 2024; Accepted: 19 December 2024
Published online: 15 January 2025

References

1. Kumar, A. et al. Sustainable and consumer-centric nanotechnology-based materials: An update on the multifaceted applications, risks and tremendous opportunities. *Nano-Struct. Nano-Obj.* **38**, 101148 (2024).
2. Jagadeesh, P., Rangappa, S. M. & Siengchin, S. Advanced characterization techniques for nanostructured materials in biomedical applications. *Adv. Ind. Eng. Polym. Res.* **7**, 122–143. https://doi.org/10.1016/j.aiepr.2023.03.002 (2024).
3. Srivastava, A. K. et al. Morphological evolution driven semiconducting nanostructures for emerging solar, biological and nanogenerator applications. *Mater. Adv.* **3**, 8030–8062 (2022).
4. Khairani, I. Y., Mínguez-Vega, G., Doñate-Buendía, C. & Gökce, B. Green nanoparticle synthesis at scale: A perspective on overcoming the limits of pulsed laser ablation in liquids for high-throughput production. *Phys. Chem. Chem. Phys.* **25**, 19380–19408 (2023).
5. Ahmed, S. F. et al. Green approaches in synthesising nanomaterials for environmental nanobioremediation: Technological advancements, applications, benefits and challenges. *Environ. Res.* **204**, 111967 (2022).
6. Kirubakaran, D. et al. In-vitro antioxidant, antidiabetic, anticholinergic activity of iron/copper nanoparticles synthesized using Strobilanthes cordifolia leaf extract. *OpenNano* **14**, 100188 (2023).
7. Samuel, M. S. et al. A review on green synthesis of nanoparticles and their diverse biomedical and environmental applications. *Catalysts* **12**, 459 (2022).
8. Chopra, H. et al. Green metallic nanoparticles: Biosynthesis to applications. *Front. Bioeng. Biotechnol.* https://doi.org/10.3389/fbioe.2022.874742 (2022).
9. Khan, et al. Monotheca buxifolia driven synthesis of zinc oxide nano material its characterization and biomedical applications. *Micromachines* **13**, 668 (2022).

10. Girigoswami, A. et al. Beneficial effects of bioinspired silver nanoparticles on zebrafish embryos including a gene expression study. *ADMET DMPK* **12**, 177–192 (2024).
11. Sidhu, A. K., Verma, N. & Kaushal, P. Role of biogenic capping agents in the synthesis of metallic nanoparticles and evaluation of their therapeutic potential. *Front. Nanotechnol.* **3**, 801620 (2022).
12. Abdullah, et al. Novel biosynthesis, characterization and bio-catalytic potential of green algae (Spirogyra hyalina) mediated silver nanomaterials. *Saudi J. Biol. Sci.* **29**, 411–419 (2022).
13. Khan, M. A. R. et al. A review on gold nanoparticles: Biological synthesis, characterizations, and analytical applications. *Results Chem.* **4**, 100478 (2022).
14. Ghobashy, M. M., Alkhursani, S. A., Alqahtani, H. A., El-damhougy, T. K. & Madani, M. Gold nanoparticles in microelectronics advancements and biomedical applications. *Mater. Sci. Eng.: B* **301**, 117191 (2024).
15. Santhosh, P. B., Genova, J. & Chamati, H. Green synthesis of gold nanoparticles: An eco-friendly approach. *Chemistry* **4**, 345–369 (2022).
16. Taha, A., Farooq, N. & Hashmi, A. A. Medicinal plant-mediated nanomaterials. In *Green Synthesis of Nanomaterials: Biological and Environmental Applications* (eds Chakravarty, A. et al.) 22–45 (Wiley, 2024). https://doi.org/10.1002/9781119900931.ch2.
17. Padalia, H. & Chanda, S. Antioxidant and anti-cancer activities of gold nanoparticles synthesized using aqueous leaf extract of *Ziziphus nummularia*. *BioNanoScience* **11**, 281–294 (2021).
18. Sher, N., Ahmed, M. & Mushtaq, N. Plant-based synthesis of AuNPs using *Hippeastrum hybridum* (L.): Their ex vivo anti-acetylcholinesterase property. *BioNanoScience* **13**, 1766–1778 (2023).
19. Raja, S. A. et al. Green synthesised AuNps using Ajuga Bracteosa extract and AuNps-Free supernatant exhibited equivalent antibacterial and anticancerous efficacies. *PloS One* **18**, e0282485 (2023).
20. Ameen, F., Al-Maary, K. S., Almansob, A. & AlNadhari, S. Antioxidant, antibacterial and anti-cancer efficacy of Alternaria chlamydospora-mediated gold nanoparticles. *Appl. Nanosci.* **13**, 2233–2240 (2023).
21. Jia, X. et al. Chemical and structural engineering of gelatin-based delivery systems for therapeutic applications: A review. *Biomacromolecules* **25**, 564–589 (2024).
22. Abar, E. S., Vandghanooni, S., Torab, A., Jaymand, M. & Eskandani, M. A comprehensive review on nanocomposite biomaterials based on gelatin for bone tissue engineering. *Int. J. Biol. Macromol.* **254**, 127556 (2024).
23. Yu, H. et al. Multifunctional porous poly (L-lactic acid) nanofiber membranes with enhanced anti-inflammation, angiogenesis and antibacterial properties for diabetic wound healing. *J. Nanobiotechnol.* **21**, 110 (2023).
24. Zhao, X. et al. Crystallization behaviors regulations and mechanical performances enhancement approaches of polylactic acid (PLA) biodegradable materials modified by organic nucleating agents. *Int. J. Biol. Macromol.* **233**, 123581 (2023).
25. Chong, W. J. et al. Biodegradable PLA-ZnO nanocomposite biomaterials with antibacterial properties, tissue engineering viability, and enhanced biocompatibility. *Smart Mater. Manuf.* **1**, 100004 (2023).
26. Akter, Y. et al. Silver nanoparticle reinforced polylactic acid and gelatin composite films for advanced wound dressing. *J. Biomater. Appl.* **38**, 915–931 (2024).
27. Lu, Q.-L., Wu, J., Wang, H., Huang, B. & Zeng, H. Plant-inspired multifunctional fluorescent cellulose nanocrystals intelligent nanocomposite hydrogel. *Int. J. Biol. Macromol.* **249**, 126019 (2023).
28. Utharalakshmi, N., Gayathri, S., Hansika, S. & Narendrakumar, G. Unlocking the therapeutic potential of *Syzygium cumini* Seeds extract. *Curr. Trends Biotechnol. Pharm.* **14**, 403–414 (2020).
29. Kumar, M. et al. Jamun (*Syzygium cumini* (L.) Skeels) Seed: A review on nutritional profile, functional food properties, health-promoting applications, and safety aspects. *Processes* **10**, 2169 (2022).
30. Chhikara, N. et al. Bioactive compounds and pharmacological and food applications of *Syzygium cumini*—A review. *Food Funct.* **9**, 6096–6115 (2018).
31. Amir Rawa, M. S., Mazlan, M. K. N., Ahmad, R., Nogawa, T. & Wahab, H. A. Roles of Syzygium in anti-cholinesterase, anti-diabetic, anti-inflammatory, and antioxidant: From Alzheimer's perspective. *Plants* **11**, 1476 (2022).
32. Mekky, A. E. et al. Bio-fabrication of silver nanoparticles using Antioxidants-rich *Syzygium cumin* L. leaves extract with the evaluation of its antibacterial, and anti-inflammatory activity. *Al-Azhar J. Agric. Res.* **48**, 460–474 (2023).
33. Aher, H., Han, S., Vikhe, A. & Kuchekar, S. Green synthesis of copper nanoparticles using *Syzygium Cumin* leaf extract, characterization and antimicrobial activity. *Chem. Sci. Trans.* **8**, 1–6 (2019).
34. Arumugam, M. et al. Green synthesis of zinc oxide nanoparticles (ZnO NPs) using Syzygium cumini: Potential multifaceted applications on antioxidants, cytotoxic and as nanonutrient for the growth of Sesamum indicum. *Environ. Technol. Innov.* **23**, 101653 (2021).
35. Suarasan, et al. Doxorubicin-incorporated nanotherapeutic delivery system based on gelatin-coated gold nanoparticles: Formulation, drug release, and multimodal imaging of cellular internalization. *ACS Appl. Mater. Interfaces* **8**, 22900–22913 (2016).
36. Rajesh, T. P. et al. The iron oxide/polymer nanocomposites for targeted drug delivery and toxicity investigation on zebra fish (*Danio rerio*). *Inorg. Chem. Commun.* **125**, 108447 (2021).
37. Bawazeer, S. et al. Black pepper (Piper nigrum) fruit-based gold nanoparticles (BP-AuNPs): Synthesis, characterization, biological activities, and catalytic applications–A green approach. *Green Process. Synth.* **11**, 11–28 (2022).
38. Muthukumar, T., Sambandam, B., Aravinthan, A., Sastry, T. P. & Kim, J.-H. Green synthesis of gold nanoparticles and their enhanced synergistic antitumor activity using HepG2 and MCF7 cells and its antibacterial effects. *Process Biochem.* **51**, 384–391 (2016).
39. Veeramani, S. et al. Nigella sativa flavonoids surface coated gold NPs (Au-NPs) enhancing antioxidant and anti-diabetic activity. *Process Biochem.* **114**, 193–202 (2022).
40. Mubeen, B. et al. Phytochemicals mediated synthesis of AuNPs from *Citrullus colocynthis* and their characterization. *Molecules* **27**, 1300 (2022).
41. Timoszyk, A. & Grochowalska, R. Mechanism and antibacterial activity of gold nanoparticles (AuNPs) functionalized with natural compounds from plants. *Pharmaceutics* **14**, 2599 (2022).
42. Alkhathlan, A. H. et al. Evaluation of the anti-cancer activity of phytomolecules conjugated gold nanoparticles synthesized by aqueous extracts of *Zingiber officinale* (ginger) and *Nigella sativa* L. seeds (black cumin). *Materials* **14**, 3368 (2021).
43. Shirzadi-Ahodashti, M. et al. Optimization and evaluation of anti-cancer, antifungal, catalytic, and antibacterial activities: Biosynthesis of spherical-shaped gold nanoparticles using Pistacia vera hull extract (AuNPs@ PV). *Arab. J. Chem.* **16**, 104423 (2023).
44. Al-Radadi, N. S. Biogenic proficient synthesis of (Au-NPs) via aqueous extract of Red Dragon Pulp and seed oil: Characterization, antioxidant, cytotoxic properties, anti-diabetic anti-inflammatory, anti-Alzheimer and their anti-proliferative potential against cancer cell lines. *Saudi J. Biol. Sci.* **29**, 2836–2855 (2022).
45. Rajkumar, M. et al. Green synthesis of gelatin-loaded magnesium hydroxide nanocomposite biomaterial using Coleus amboinicus leaf extract for enhanced antibacterial, antioxidant, anticholinergic, and wound healing activities. *J. Mater. Res.* **39**, 548–564 (2024).
46. Durmuş, S. et al. Synthesis, characterization, and in vitro drug release properties of AuNPs/p (AETAC-co-VI)/Q nanocomposite hydrogels. *Gold Bull.* **54**, 75 (2021).
47. Jomova, K. et al. Reactive oxygen species, toxicity, oxidative stress, and antioxidants: Chronic diseases and aging. *Arch. Toxicol.* **97**, 2499–2574 (2023).

48. Shah, et al. Engineering novel gold nanoparticles using *Sageretia thea* leaf extract and evaluation of their biological activities. *J. Nanostruct. Chem.* **12**, 129–140 (2022).
49. He, J. et al. Cold stress regulates accumulation of flavonoids and terpenoids in plants by phytohormone, transcription process, functional enzyme, and epigenetics. *Crit. Rev. Biotechnol.* **43**, 680–697 (2023).
50. Alam, M. W. et al. Effect of Mo doping in NiO nanoparticles for structural modification and its efficiency for antioxidant, antibacterial applications. *Sci. Rep.* **13**, 1328 (2023).
51. Dubey, S. et al. Breaking barriers in eco-friendly synthesis of plant-mediated metal/metal oxide/bimetallic nanoparticles: Antibacterial, anti-cancer, mechanism elucidation, and versatile utilizations. *J. Nanomater.* **2024**, 9914079 (2024).
52. Zafar, S. et al. Development of iron nanoparticles (FeNPs) using biomass of enterobacter: Its characterization, antimicrobial, anti-Alzheimer's, and enzyme inhibition potential. *Micromachines* **13**, 1259 (2022).
53. Dharmalingam, K. et al. Biogenic synthesis of copper nanoparticle using impatiens *Chinensis* L.: Insights into antimicrobial, antioxidant and anti-cancer activity. *J. Mol. Struct.* **1317**, 138991. https://doi.org/10.1016/j.molstruc.2024.138991 (2024).
54. Jayanetti, M. et al. In vitro influence of PEG functionalized ZnO–CuO nanocomposites on bacterial growth. *Sci. Rep.* **14**, 1293. https://doi.org/10.1038/s41598-024-52014-6 (2024).
55. He, R., Zhou, D., Xiao, L. & Li, Y. Chlorella vulgaris extract-decorated gold nanoparticle hybridized antimicrobial hydrogel as a potential dressing. *Gels* **9**, 11 (2023).
56. Baskaran Stephen, I., Bang-Yuan, C., Chia-Wei, L. & Bing-Huei, C. Green synthesis, characterization and evaluation of catalytic and antibacterial activities of chitosan, glycol chitosan and poly(γ-glutamic acid) capped gold nanoparticles. *Int. J. Biol. Macromol.* **161**, 1484–1495. https://doi.org/10.1016/j.ijbiomac.2020.07.244 (2020).
57. Ullah, et al. In vitro and in vivo applications of *Euphorbia wallichii* shoot extract-mediated gold nanospheres. *Green Process. Synth.* **10**, 101–111 (2021).
58. Mandapalli, P. K. et al. Polymer–gold nanoparticle composite films for topical application: Evaluation of physical properties and antibacterial activity. *Polym. Compos.* **38**, 2829–2840. https://doi.org/10.1002/pc.23885 (2017).
59. Fernandes, A., Rodrigues, P. M., Pintado, M. & Tavaria, F. K. A systematic review of natural products for skin applications: Targeting inflammation, wound healing, and photo-aging. *Phytomedicine* **115**, 154824. https://doi.org/10.1016/j.phymed.2023.154824 (2023).
60. Murugan, et al. Nanoformulated CPMSN biomaterial regulates proinflammatory cytokines to heal wounds and kills drug-resistant bacteria. *Curr. Sci.* **118**, 1583–1591 (2020).
61. Jan, et al. Plant-based synthesis of zinc oxide nanoparticles (ZnO-NPs) using aqueous leaf extract of *Aquilegia pubiflora*: Their antiproliferative activity against HepG2 cells inducing reactive oxygen species and other in vitro properties. *Oxid. Med. Cell. Long.* **1**, 4786227 (2021).
62. Wautier, J.-L. & Wautier, M.-P. Pro- and anti-inflammatory prostaglandins and cytokines in humans: A mini review. *Int. J. Mol. Sci.* **24**, 9647 (2023).
63. Mishra, A. K. et al. Nanoinformatics and nanotechnology in anti-inflammatory therapy: A review. *J. Drug Deliv. Sci. Technol.* **93**, 105446. https://doi.org/10.1016/j.jddst.2024.105446 (2024).
64. Ojo, O. A., Ibrahim, H. S., Rotimi, D. E., Ogunlakin, A. D. & Ojo, A. B. Diabetes mellitus: From molecular mechanism to pathophysiology and pharmacology. *Med. Nov. Technol. Devices* **19**, 100247. https://doi.org/10.1016/j.medntd.2023.100247 (2023).
65. Ghosh, N. et al. Exploring the complex relationship between diabetes and cardiovascular complications: Understanding diabetic cardiomyopathy and promising therapies. *Biomedicines* **11**, 1126 (2023).
66. Gómez-Maqueo, A., Ferreira-Lazarte, A., Amirruddin, N. S. & Lin, A.H.-M. Generating slow digestibility in cooked potatoes by modulating starch accessibility to α-amylase and mucosal α-glucosidase to different levels. *Food Hydrocoll.* **141**, 108718. https://doi.org/10.1016/j.foodhyd.2023.108718 (2023).
67. Faisal, S. et al. In vivo analgesic, anti-inflammatory, and anti-diabetic screening of *Bacopa monnieri*-synthesized copper oxide nanoparticles. *ACS omega* **7**, 4071–4082 (2022).
68. Prabakaran, K. & Govindan, S. Antidiabetic activity and phytochemical constituents of *Syzygium cumini* Seeds in Puducherry Region, South India. *Int. J. Pharmacogn. Phytochem. Res.* https://doi.org/10.25258/phyto.v9i07.11168 (2017).
69. Faisal, et al. Curcuma longa mediated synthesis of copper oxide, nickel oxide and Cu-Ni bimetallic hybrid nanoparticles: Characterization and evaluation for antimicrobial, anti-parasitic and cytotoxic potentials. *Coatings* **11**, 849 (2021).
70. Perluigi, A. et al. Oxidative damage in neurodegeneration: Roles in the pathogenesis and progression of Alzheimer disease. *Physiol. Rev.* **104**, 103–197. https://doi.org/10.1152/physrev.00030.2022 (2024).
71. Rajkumar, A. et al. Galantamine tethered hydrogel as a novel therapeutic target for streptozotocin-induced Alzheimer's disease in Wistar rats. *Curr. Res. Pharmacol. Drug Discov.* **3**, 100100 (2022).
72. Girgin, M., Isik, S. & Kantarci-Carsibasi, N. Proposing novel natural compounds against Alzheimer's disease targeting acetylcholinesterase. *PLoS One* **18**, e0284994. https://doi.org/10.1371/journal.pone.0284994 (2023).
73. Imran, M. et al. In vitro examination of anti-parasitic, anti-Alzheimer, insecticidal and cytotoxic potential of Ajuga bracteosa Wallich leaves extracts. *Saudi J. boil. Sci.* **28**, 3031–3036 (2021).
74. İpek, P. et al. Green synthesis and evaluation of antipathogenic, antioxidant, and anticholinesterase activities of gold nanoparticles (Au NPs) from *Allium cepa* L. peel aqueous extract. *Biomass Convers. Biorefinery* **14**, 10661–10670. https://doi.org/10.1007/s13399-023-04362-y (2024).
75. Zainab, A. et al. Green synthesis, characterization and cholinesterase inhibitory potential of gold nanoparticles. *J. Mex. Chem. Soc.* https://doi.org/10.29356/jmcs.v65i3.1479 (2021).
76. Ryu, J., Girigoswami, K., Ha, C., Ku, S. H. & Park, C. B. Influence of multiple metal ions on β-amyloid aggregation and dissociation on a solid surface. *Biochemistry* **47**, 5328–5335 (2008).
77. Ha, C., Ryu, J. & Park, C. B. Metal ions differentially influence the aggregation and deposition of Alzheimer's β-amyloid on a solid template. *Biochemistry* **46**, 6118–6125 (2007).
78. Barbalinardo, M. et al. Effect of metallic nanoparticles on amyloid fibrils and their influence to neural cell toxicity. *Nano Research* **13**, 1081–1089 (2020).
79. Wang, J., Feng, Y., Tian, X., Li, C. & Liu, L. Disassembling and degradation of amyloid protein aggregates based on gold nanoparticle-modified g-C3N4. *Colloids Surf. B: Biointerf.* **192**, 111051 (2020).
80. De Conto, V. et al. In vitro differentiation modifies the neurotoxic response of SH-SY5Y cells. *Toxicol. Vitro* **77**, 105235. https://doi.org/10.1016/j.tiv.2021.105235 (2021).
81. Singh, A. K. Comparative therapeutic effects of plant-extract synthesized and traditionally synthesized gold nanoparticles on alcohol-induced inflammatory activity in SH-SY5Y cells in vitro. *Biomedicines* **5**, 70 (2017).
82. Venkatesh, G. et al. Green synthesis, characterization, anti-cancer and antimicrobial activity of AuNPs extracted from *Euphorbia antiquorum* stem and flower: Experimental and theoretical calculations. *J. Drug Deliv. Sci. Technol.* **95**, 105583. https://doi.org/10.1016/j.jddst.2024.105583 (2024).
83. Udayakumar, S. et al. Exploring the amyloid degradation potential of nanoformulated carrageenan-bridging in vitro and in vivo perspectives. *Int. J. Biol. Macromol.* **279**, 134814. https://doi.org/10.1016/j.ijbiomac.2024.134814 (2024).
84. Girigoswami, A., Deepika, B., Pandurangan, A. K. & Girigoswami, K. Preparation of titanium dioxide nanoparticles from *Solanum Tuberosum* peel extract and its applications. *Artif. Cells Nanomed. Biotechnol.* **52**, 59–68 (2024).

85. Günter, E. A., Melekhin, A. K., Belozerov, V. S., Martinson, E. A. & Litvinets, S. G. Preparation, physicochemical characterization and swelling properties of composite hydrogel microparticles based on gelatin and pectins with different structure. *Int. J. Biol. Macromol.* **258**, 128935. https://doi.org/10.1016/j.ijbiomac.2023.128935 (2024).
86. Moreno-Bautista, G. & Tam, K. C. Evaluation of dialysis membrane process for quantifying the in vitro drug-release from colloidal drug carriers. *Colloids Surf. A: Physicochem. Eng. Aspects* **389**, 299–303. https://doi.org/10.1016/j.colsurfa.2011.07.032 (2011).
87. Christodouleas, D. C., Fotakis, C., Nikokavoura, A., Papadopoulos, K. & Calokerinos, A. C. Modified DPPH and ABTS assays to assess the antioxidant profile of untreated oils. *Food Anal. Methods* **8**, 1294–1302. https://doi.org/10.1007/s12161-014-0005-6 (2015).
88. Miller, et al. Factors influencing the antioxidant activity determined by the ABTS·+ radical cation assay. *Free Radical Res.* **26**, 195–199 (1997).
89. Sroka, Z. & Cisowski, W. Hydrogen peroxide scavenging, antioxidant and anti-radical activity of some phenolic acids. *Food Chem. Toxicol.* **41**, 753–758. https://doi.org/10.1016/S0278-6915(02)00329-0 (2003).
90. Zhao, H., Zhang, R., Yan, X. & Fan, K. Superoxide dismutase nanozymes: An emerging star for anti-oxidation. *J. Mater. Chem. B* **9**, 6939–6957. https://doi.org/10.1039/d1tb00720c (2021).
91. Pulido, R., Bravo, L. & Saura-Calixto, F. Antioxidant activity of dietary polyphenols as determined by a modified ferric reducing/antioxidant power assay. *J. Agric. Food Chem.* **48**, 3396–3402. https://doi.org/10.1021/jf9913458 (2000).
92. Ou, B., Huang, D., Hampsch-Woodill, M., Flanagan, J. A. & Deemer, E. K. Analysis of antioxidant activities of common vegetables employing oxygen radical absorbance capacity (ORAC) and ferric reducing antioxidant power (FRAP) assays: A comparative study. *J. Agric. Food Chem.* **50**, 3122–3128. https://doi.org/10.1021/jf0116606 (2002).
93. Jahangirian, H. et al. Well diffusion method for evaluation of antibacterial activity of copper phenyl fatty hydroxamate synthesized from canola and palm kernel oils. *Digest J. Nanomater. Biostruct.* **8**, 1263–1270 (2013).
94. Harrak, Y. et al. Synthesis, anti-inflammatory activity, and in vitro antitumor effect of a novel class of cyclooxygenase inhibitors: 4-(Aryloyl)phenyl methyl sulfones. *J. Med. Chem.* **53**, 6560–6571. https://doi.org/10.1021/jm100398z (2010).
95. Thilagam, E., Parimaladevi, B., Kumarappan, C. & Chandra Mandal, S. α-glucosidase and α-amylase inhibitory activity of senna surattensis. *J. Acupunct. Meridian Stud.* **6**, 24–30. https://doi.org/10.1016/j.jams.2012.10.005 (2013).
96. Šinko, G., Čalić, M., Bosak, A. & Kovarik, Z. Limitation of the Ellman method: Cholinesterase activity measurement in the presence of oximes. *Anal. Biochem.* **370**, 223–227. https://doi.org/10.1016/j.ab.2007.07.023 (2007).
97. Asghar, A. et al. Synthesis, acetylcholinesterase (AChE) and butyrylcholinesterase (BuChE) activities, and molecular docking studies of a novel compound based on combination of flurbiprofen and isoniazide. *RSC Adv.* **10**, 19346–19352. https://doi.org/10.1039/d0ra02339f (2020).
98. Deepika, B., Pallavi, P., Gowtham, P., Girigoswami, A. & Girigoswami, K. Anti-cancer potential of nanoformulated extract of *Passiflora incarnata* leaves. *Biocatal. Agric. Biotechnol.* **57**, 103109 (2024).
99. Harini, K. et al. Niosomal bupropion: Exploring therapeutic frontiers through behavioral profiling. *Pharmaceuticals* **17**, 366 (2024).
100. Rajkumar, M. et al. Gelatin/polyvinyl alcohol loaded magnesium hydroxide nanocomposite attenuates neurotoxicity and oxidative stress in Alzheimer's disease induced rats. *Int. J. Biol. Macromol.* **222**, 2122–2143 (2022).

Acknowledgements

This work was financially supported by a Senior Research Fellowship (SRF) from SSN College of Engineering, Chennai-603 110, Tamil Nadu, India (SSN/CE/SRF/2024). The authors are thankful to the Researchers Supporting Project Number (RSPD2025R940), King Saud University, Riyadh, Saudi Arabia for supporting this study. J acknowledges Chettinad Academy of Research and Education for providing PhD fellowship. We acknowledge the support of Dr.Prakruti Joshi, Department of Language, Ganpat University for providing her critical input in correcting the language of this manuscript.

Author contributions

Manickam Rajkumar: Methodology, Investigation, Writing—review and editing, Funding, Writing—original draft. S.I. Davis Presley: Supervision, Investigation, Data collection, Conceptualization. Nathiya Thiyagarajulu: Data collection, Formal analysis; Koyeli Girigoswami: Data collection, Formal analysis; Gopalarethinam Janani: Data correction, Formal analysis; Chinnaperumal Kamaraj: Software analysis, Formal analysis. Bharathi Madheswaran: Methodology, Software analysis; Bhupendra Prajapati: Data correction, Software analysis; Nemat Ali: Software analysis, Formal analysis; Mohammad Rashid Khan: Funding, Formal analysis.

Declarations

Competing interests

The authors declare that they have no known competing financial interests or personal relationships that could have appeared to influence the work reported in this paper.

Consent for publication

All the authors agreed to publish the data in this journal.

Additional information

Supplementary Information The online version contains supplementary material available at https://doi.org/10.1038/s41598-024-84098-5.

Correspondence and requests for materials should be addressed to S.I.D.P. or K.G.